Ore Geology Reviews 153 (2023) 105280

Contents lists available at ScienceDirect

Ore Geology Reviews

journal homepage: www.elsevier.com/locate/oregeorev

The geochronology of the rare metal pegmatite deposits: A case study in Nanping No. 31 pegmatite vein in northeastern Cathaysian block, China

Wang Hao-Yu [a,b], Tang Yong [a,*], Zhang Hui [a], Lv Zheng-Hang [a], Xu Yu-Sheng [a,b]

[a] Key Laboratory for High Temperature and High-Pressure Study of the Earth's Interior, Institute of Geochemistry, Chinese Academy of Sciences, Guiyang 550002, China
[b] University of Chinese Academy of Sciences, Beijing 100049, China

ARTICLE INFO

Keywords:
Geochronology
Nanping pegmatite
U–Pb dating
Apatite
Cassiterite
Columbite–tantalite

ABSTRACT

Accurate dating of the pegmatite is a challenge due to the uncertainty and controversy of crystallization temperature, fractionation model, and cooling mechanism. In this study, the sizable Nanping No.31 pegmatite vein (southeast China) contain five structural zones that is considered as an ideal example for assessing credible dating method on rare metals pegmatite deposit. The CMS (Chemical composition-Mineral assemblage-Structural geology) classification is applied on the Nanping pegmatite. The No. 31 vein is identified as pegmatite by CMS features. New U–Pb dating CGMs (columbite-tantalite group minerals) in five zones have a consistent age (380 ± 10 Ma). Whilst U–Pb dating of apatite and cassiterite from different structural zones show remarkable two group isotopic ages (370–390 Ma and 145–160 Ma). The much younger age indicated the pegmatite vein has experienced a severe Yanshanian tectono-thermal event at Eastern China. By comparison with apatite, cassiterite and zircon, CGMs is the most suitable mineral for accurate dating of the pegmatite because the dating results of the minerals are much stable, even having metamictization caused by high U content or overprinting by late hydrothermal activity. This study provided new insight into the dating methods for rare metals pegmatites to accurate restrict its metallogenetic geodynamical setting.

1. Introduction

Rare metals including Li, Be, Sn, Nb and Ta are critical to the emerging high-tech and green industries (e.g., electronics, solar panels, fiber optics, etc) and are considered as strategic or critical metals by many countries and organizations in the world (Hou et al., 2020; European Commission, 2020). The rare metal pegmatite deposit (enriched in Li, Rb, Cs, Be, Sn, Ta, and Nb) is a crucial rare metal deposit type (Černý et al., 2005). Accurate determining of the mineralizing age of the deposits is a crucial issue to restrict its metallogenetic geodynamical setting.

Rock-forming minerals (feldspar, muscovite), accessory minerals (zircon, apatite), and ore minerals (columbite-group minerals, cassiterite) in pegmatite can be used in geochronology studies (Tkachev et al., 2011; McCauley and Bradley, 2014; Jiang et al., 2021). However, the K–Ar, Ar–Ar, and Rb–Sr isotopic systems in the rock-forming minerals have low closure temperatures and are easily disturbed. Currently, the zircon U–Pb isotope system is the most widely used in pegmatite dating (Ren et al., 2011; Zhou et al., 2015; Ma et al., 2015; Tang et al., 2017; Lv et al., 2012, 2018a, 2018b, 2021a). Zircon in pegmatite frequently suffers from metamictization and often experiences recrystallization due to high U and Th content. It usually leads to loss of radioactive Pb in zircon crystals, resulting in younger dating results (Lv et al., 2018b). Furthermore, zircon in pegmatite have abundant mineral inclusions. These features make it challenging to constrain the geochronology of pegmatite by using the zircon U–Pb isotopic system. For example, zircon from Kelumute No.112 pegmatite in Altay, northwestern China, has complex U–Pb ages. The zircon $^{206}Pb/^{238}U$ ages from zone II alone can be divided into 234 ± 4 Ma, 215–216 Ma, and 186 ± 3 Ma (Lv et al., 2012). The geological implication of these ages is unclear.

The columbite-tantalite group minerals $[(Fe,Mn)(Nb,Ta)_2O_6]$ are critical ore minerals of niobium and tantalum in rare metal pegmatite deposit. These minerals can be used for U–Pb dating because of high U and low Pb contents (Romer and Smeds, 1994, 1996, 1997; Legros et al., 2019). CGMs U–Pb dating can constrain the emplacement age of the rocks, even though it is hard to date using zircon U–Pb isotopes (Geisler et al., 2002, 2007). Researches have indicated that the U–Pb dating of CGMS is a powerful method for dating CGMs-bearing rocks such as pegmatite (Romer and Smeds, 1996; Smith et al., 2004; Baumgartner et al., 2006; Melcher et al., 2015; Deng et al., 2013; Che et al., 2015;

* Corresponding author.
E-mail addresses: wanghaoyu@mail.gyig.ac.cn (W. Hao-Yu), tangyong@vip.gyig.ac.cn (T. Yong).

https://doi.org/10.1016/j.oregeorev.2022.105280
Received 15 August 2022; Received in revised form 26 December 2022; Accepted 29 December 2022
Available online 31 December 2022

2019; Van Lichtervelde et al., 2017; Zhou et al., 2018; Kendall-Langley et al., 2020; Feng et al., 2020). Cassiterite is the dominant tin ore mineral and commonly crystallizes in sn-rich pegmatite. Cassiterite (SnO_2) belongs to the rutile group ($M^{4+}O_2$), with moderately high U and low common Pb in its crystal structure. Its high closure temperature of 500–800 °C (Cherniak, 2006; Huntington and Klepeis, 2018), and resistance to post-mineralization hydrothermal disturbance (Zhang et al., 2017) make cassiterite U–Pb dating an effective method to date tin mineralization and cassiterite-bearing rare metal pegmatite (Yan et al., 2018; Yuan et al., 2011; Zhang et al., 2017). Apatite is a common accessory mineral in pegmatite and has been widely used in geochronology because it frequently preferentially incorporates U relative. However, compared with zircon, CGMs, and cassiterite, apatite has a relatively lower U–Pb closure temperature (350 °C–500 °C; Chamberlain and Bowring, 2000; Cherniak and Watson, 2000; Krogstad and Walker, 1994; Huntington and Klepeis, 2018) and more content of common Pb (Chew et al., 2011). Therefore, it has dating potential, but it may also be reset the age by later thermal events.

In this work, laser ablation (LA), multicollector (MC) inductively coupled plasma (ICP) mass spectrometry (MS) were used to date the above minerals from five structural zones of Nanping No.31 pegmatite vein, and also try to apply the CMS (Chemical composition-Mineral assemblage-Structural geology) classification (Dill, 2016) on the No. 31 pegmatite vein. The focus is to evaluate the applicability of different minerals to dating from different zones in pegmatite, determine the most suitable dating minerals of pegmatite, and try to constrain the geodynamic setting and consolidation rate of the pegmatite.

2. Geologic setting

The Nanping pegmatite district is in the northeastern portion of the South China Craton (SCC) (Fig. 1a). The SCC comprises the Yangtze block in the northwest and the Cathaysian Block in the southwest. The Jiangshan–Shaoxing fault is the eastern boundary of the Cathaysian and Yangtze blocks; however, the western boundary of the two blocks has not been determined (Zhao and Cawood, 2012; Zhang et al., 2015). The SCC experienced multiple Phanerozoic tectonic thermal events, resulting in angular unconformity between the Silurian–Devonian and the Triassic–Jurassic in the Cathaysian and Yangtze blocks. The Early Paleozoic orogeny comprises numerous 450–420 Ma S-type granites and medium- to high-grade metamorphism, accompanied by some basic, andesitic, and I-type granitic magmatism (Wang et al., 2013; Zhang et al., 2015). In the early Mesozoic, the SCC was affected by the Indosinian orogeny, consistent with the Early Paleozoic orogeny. Many 240–200 Ma S-type granites and a lack of contemporaneous volcanism or basic magmatism occur (Zhou et al., 2006; Shu et al., 2015). S-type granites from the above ages are directly derived from the partial melting of the Precambrian crust or only a small amount of mantle material (Shu et al., 2015).

The SCC, the Indosinian block, and the Sibumasu block collided and spliced into eastern Asia in the early Mesozoic. Therefore, the early Mesozoic orogeny reshaped the entire East Asian tectonic framework. The understanding of the SCC's Indosinian orogeny is controversial. Some scholars proposed that the collision and compression between the SCC and the surrounding blocks in the early Mesozoic formed the Indosinian orogeny in South China (Zhou et al., 2006). Other scholars suggested that the plane subduction of the paleo Pacific plate in the early

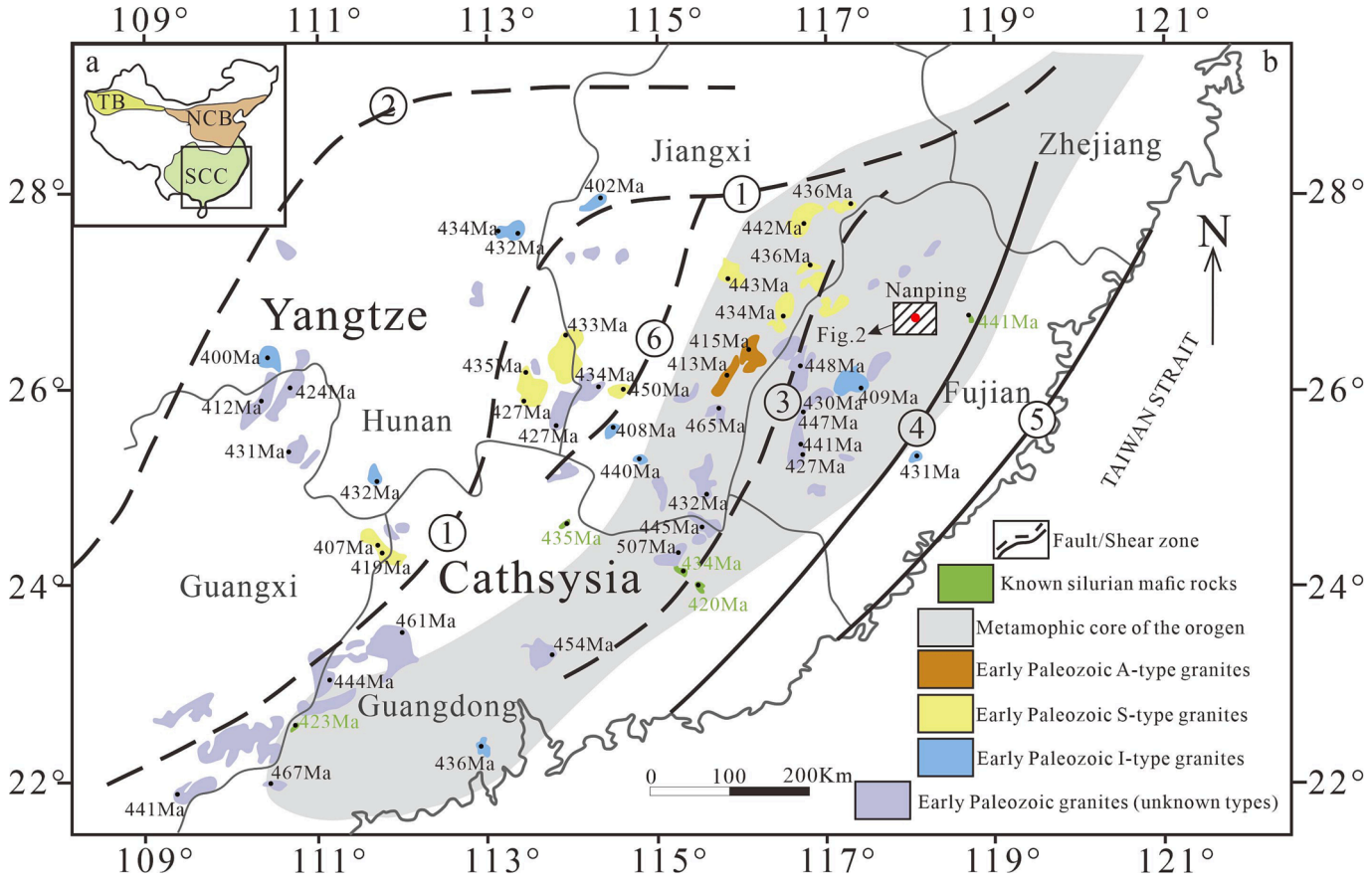

Fig. 1. Geological map with the distribution of the Early Paleozoic granitic and mafic plutons in the South China Craton (modified after Li et al., 2010a, 2010b; Wang et al., 2013; Tang et al., 2017). SCC: South China Craton; NCB: North China Block; TB: Tarim Block. Faults: (1) Shaoxing–Jiangshan–Chenzhou–Linwu Fault; (2) Anhua–Luocheng Fault; (3) Heyuan–Guangfeng Fault; (4) Zhenghe–Dapi Fault; (5) Chengle–Nan'ao Fault; (6) Ganjiang Fault.

Mesozoic caused the Indosinian orogeny in South China (Li et al., 2006; Li and Li, 2007; Li et al., 2012). The Yanshanian orogeny comprises numerous 150–110 Ma I-type granites and contemporaneous volcanism, accompanied by intense typical magmatic activity (Shu et al., 2009). It was the strongest Phanerozoic orogeny experienced in the SCC, closely related to the subduction of the Pacific plate to Eurasia (Zhou et al., 2006; Li et al., 2014).

3. Geology of the Nanping No.31 pegmatite vein

The exposed strata of Nanping pegmatite province are Proterozoic metamorphic, Upper Neoproterozoic to Ordovician shallow metamorphic sediments, Upper Paleozoic to lower Middle Triassic rock sequence, Mesozoic Cenozoic volcanic rocks, and sediments. Folds and faults are developed in the Nanping pegmatite district, in which folds are primarily developed in a metamorphic basement with a predominant N–NE strike and faults are dominated N—S (Fig. 2).

More than 500 pegmatite veins are distributed in the Nanping pegmatite province, with an exposed area of over 250 km^2. The mineral assemblage and mineralization features of the Nanping pegmatites are summarized in Tang et al., 2017. The No.31 pegmatite is the highest differentiated and best rare-metal mineralization, and its scale has reached the super-large Nb–Ta–Sn deposit. According to reserve explorations, this vein contains approximately 260 tons of Nb_2O_5, with an average grade of 0.016 wt%, and approximately 440 tons of Ta_2O_5, with an average grade of 0.028 wt% (https://www.fjsq.gov.cn). Tang et al (2017) investigated the chronology of columbite-(Fe) and zircon from zone I in Nanping No.31 pegmatite by LA-ICP-MS U–Pb dating and revealed that the emplacement age of the Nanping pegmatites occurred at approximately 387 Ma.

The No.31 pegmatite (118°06′N, 26°40′E) is a lenticular body, trending N–NE, 300–600 m long, maximal 5–6 m thick, and approximately 90 m wide. It is steeply intruded into the schist and granulite of the Xiafeng formation of the Middle Neoproterozoic whole-rock group (Fig. 3a). Fig. 3b shows that Qiu and Yang (1985) divided the No.31 pegmatite vein into five mineral symbiotic structural zones from the edge to the core according to its structure and mineral composition: Zone I comprises quartz (40–60 vol%), muscovite (30–40 vol%), and albite (10–25 vol%), forming a discontinuous thin shell distributed at the vein's edge. The primary rare-metal minerals in the zone are cassiterite, Nb-Fe-columbite, zircon, and beryl. Zone II typically contains greenish muscovite and saccharoidal albite, distributed discontinuously in zone I or in direct contact with zone V and IV. It can be further divided into two substructure zones (II_a and II_b). Zone II_a comprises saccharoidal albite (over 90 vol%), and II_b contains quartz (10 vol%), albite (30 vol%), and green muscovite (50 vol%). Numerous melanocratic minerals (cassiterite, niobium iron group minerals, and tin-bearing Mn-tantalite) crystallize between the transition zones of II_a and II_b. Zone III primarily comprises cleavelandite and coarse quartz. Spodumene crystallizes on the inner side, with small amounts of muscovite, amblygonite-montebrasite, columbite–tantalite-group minerals, tungsten–niobium-group minerals, zircon, cassiterite, fluoroapatite, and beryl. Zone IV is in the middle of a pegmatite vein and primarily contains coarse quartz and spodumene. Numerous Nb, Ta, Sn minerals, and beryl are formed after phosphate metasomatism, filled between massive quartz and spodumene in this zone. Zone V (quartz core) comprises blocky quartz and K-feldspar, and accessory minerals are invisible.

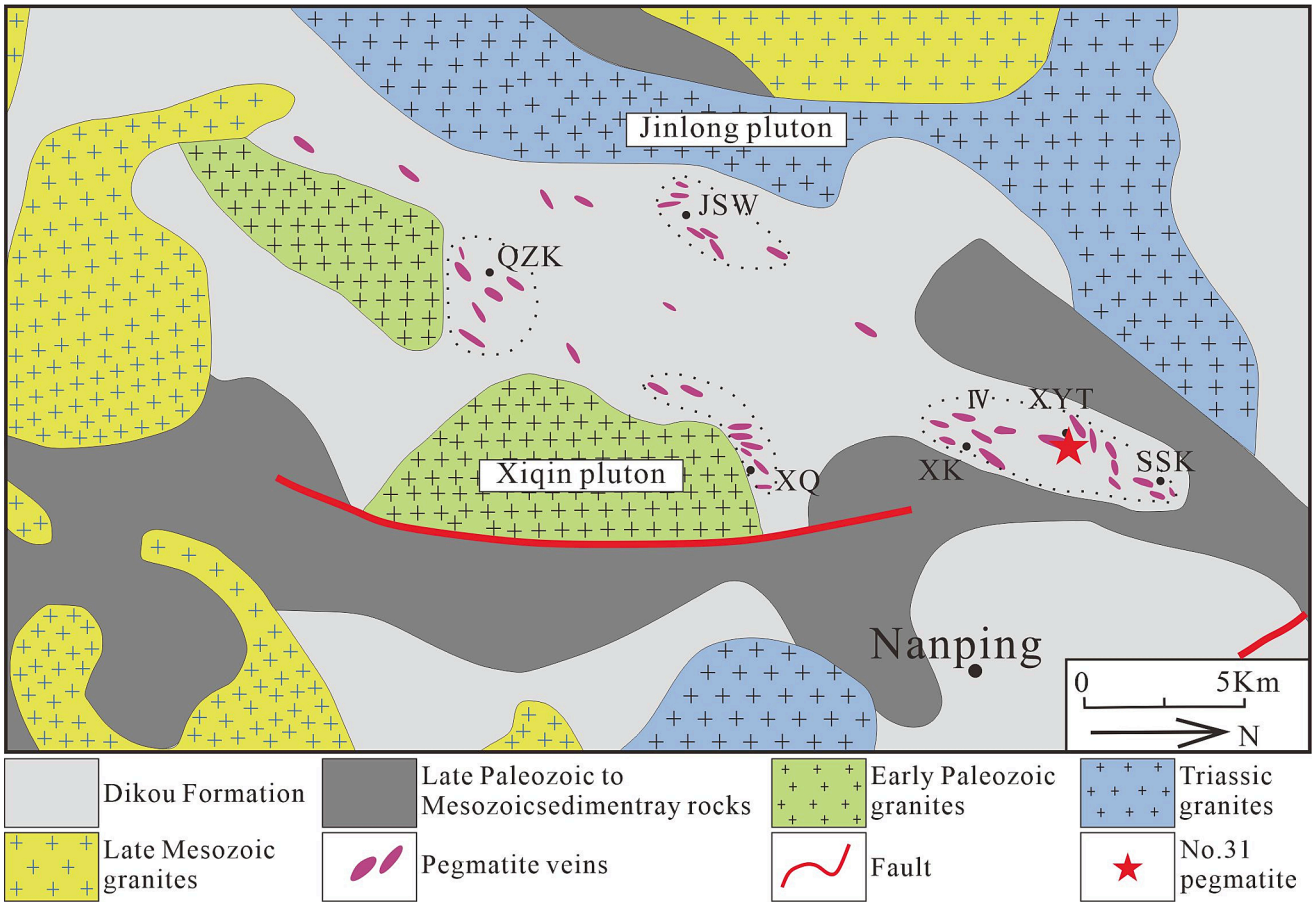

Fig. 2. Simplified geological map of the Nanping pegmatite district (modified after Yang et al., 1987; Tang et al., 2017). SSK: Shishunken; XYT: Xiyuantou; XK: Xiken; XQ: Xiqin; JSW: Jushuwang; QZK: Qiuzhuke.

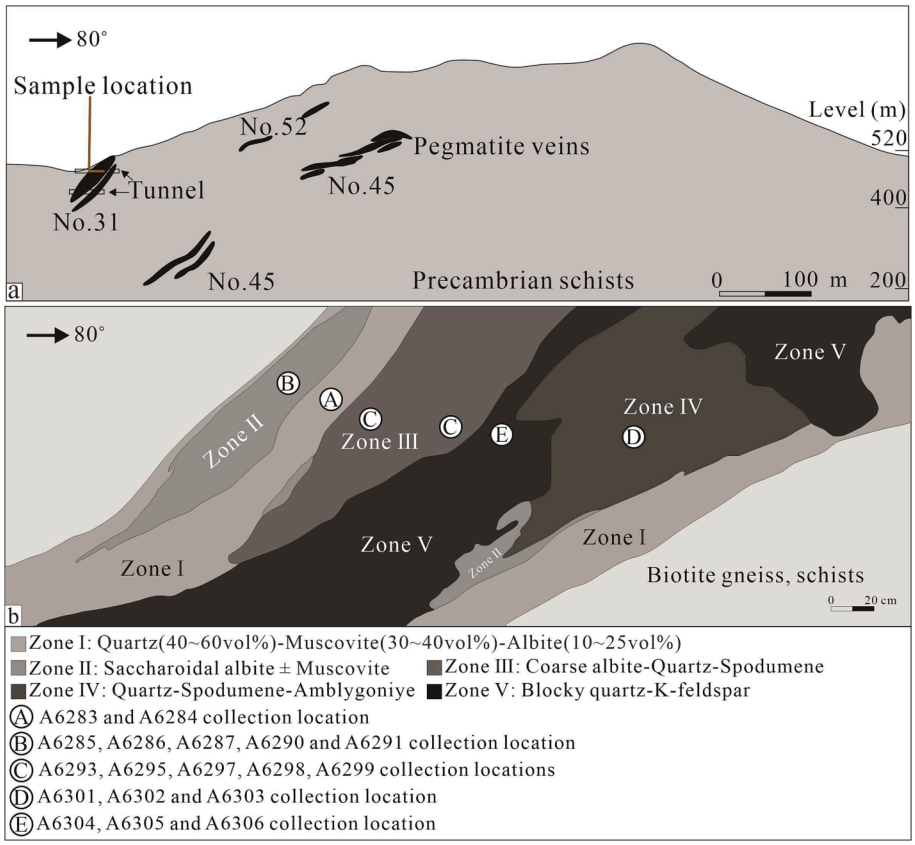

Fig. 3. The (a) profile and (b) internal textural zones of the Nanping No.3 granitic pegmatite vein (modified after Yang et al., 1987; Tang et al., 2017). The (b) is the plan of pegmatite according to the tunnels.

The Xiqin and Jinlong granites limit the distribution of these pegmatite veins (Fig. 2). Cai (2017) reported the age of Xiqin and Jinlong granites, which are 410 Ma and 220 Ma respectively. The difference in age and zircon Hf isotopic composition excludes the genetic relationship between Xiqin, Jinlong granites and Nanping pegmatite (Cai et al., 2016; Cai, 2017; Tang et al., 2017). The geodynamic setting of the

Table 1
The CMS classification of the pegmatitic rocks from the Cathaysian Block (Nanping and Fanjingshan) and Chinese Altay.

Geodynamic unit	Pegmatitc locations	Shape and structure	Contact relationship	Mineral association	Host rocks	Chemical qualifier	Type	Geodynamic setting	reference
Cathaysian Block	Nanping-Xikeng-Xiqin	Vein-type lens pocket; a few to hundreds of meters in length, and several to thirty meters in thickness	Sharp	Quartz-muscovite-albite; saccharoidal ablite; cleavelandite-K-feldspar; cassiterite, columbite-tantalite, beryl, spodumene, apatite	Biotite gneiss, schist	Sn-Nb-Ta-P-Be-Li	Pegmatite	High temperature, low pressure, and relatively stable, may be post-orogenic extensional	Cai et al., 2016; Tang et al., 2016; Yang et al., 2003
Cathaysian Block, Jiangnan Orogen	Taoshulin-Mocaogou	Tabular shape with a length and thickness of about 1900 m and 0.2–7 m, respectively	Sharp	Quartz-microcline-muscovite-albite-schorl; columbite-(Mn), cassiterite, lepidolite	Slates, mafic volcanic rock and granite	Li-P-B-sn-Ta-Nb	Granitic pegmatite	Post-orogenic extension	Lv et al., 2021b
Qiongkuer domain	Aweitan Kuertu Tiemulete Nalinsala	Veinlet pocket Schlieren arborization	Gradual	K-Ca feldspar, quartz, muscovite, tourmaline-(Fe), apatite-(F), magnetite, ilmenite, rutile, almandine, kyanite, epidote	Migmatite, gneiss	F-B; F-P-B; REE-Nb-F	Pegmatoid *meta*-pegmatoid	Synorogenic stage	Lv et al., 2018b
Kelang basin, Qiongkuer domain	Liangkeshu	Lens	Sharp	Ca-K feldspar, quartz, muscovite, magnetite, pyrite, almandine, pyrope, epidote	Quartz-biotite, schist and monzonitic granite	Mn-Mg-Fe	Pseudo-pegmatite	Forearc extensional basin during subduction	Jiang, 2012; Lv et al., 2018b

Nanping pegmatite is unclear. According to the CMS features of Nanping No. 31 pegmatite (rich in Nb-Ta-sn-Be-Li; Table 1), if there is no deep parent granite of pegmatite, the Nanping pegmatite may be generated by anatexis of the metasedimentary rocks under a post-accretion extensional setting (Dill, 2015; Cai, 2017). More accurate geodynamic setting of Nanping pegmatite requires more research to constrain.

4. Samples and methodology

The sample locations are remarked in Fig. 3b. Despite the accessory minerals are invisible in some zones of pegmatite, such as in zone V. Apatite, cassiterite and CGMs are still obtained by collecting typical bulk samples in the zone, crushing and flotation. Then, they were mounted separately in the epoxy resin, and polished until the grain interiors were exposed using standard methods. Due to the emplacement age of the Nanping No. 31 pegmatite has reported by Tang et al., 2017, we use all Concordance data as the result to obtain the weighted mean age rather than Concordia age in order to objectively show the application, limitation, and accuracy of various methods in different zones. Besides, the data of all zircon and CGMs in Zone I are from Tang et al., 2017 and Cai, 2017.

Transmitted-light images, reflected-light images, and electron backscattered diffraction (BSE) images of apatite, cassiterite, and CGMs were used to avoid the ablation of mineral inclusions during the LA-ICP-MS. Before LA-ICP-MS analysis, an energy dispersive spectrometer (EDS) was used to analyze the major elements to ensure the accuracy of the target mineral selection. For the in-situ U–Pb analysis, all samples were ablated using a Geo-Laspro 193 nm ArF excimer laser (CompexPro 102F, Coherent) coupled to a Thermo Scientific Element XR sector field ICP-MS at the State Key Laboratory of Ore Deposit Geochemistry (SKLODG), Institute of Geochemistry, Chinese Academy of Sciences (IGCAS), Guiyang, China.

4.1. Apatite, cassiterite and CGMs BSE cathodoluminescence (CL) EDS

Scanning electron microscopy (SEM) BSE-CL images of apatite, cassiterite, and CGMs were obtained at the State Key Laboratory of Nuclear Resources and Environment, East China University of Technology (Nanchang, Jiangxi), using a Zeiss Gemini Sigma 300 VP scanning electron microscope equipped with a CL detector. An acceleration voltage of 15 kV, a probe current of ~ 6nA, and a magnification of ~ 100 to 300x were used.

4.2. Apatite U–Pb dating

Apatite U–Pb isotopic analyses were performed at the SKLODG, IGCAS using a GeoLas Pro 193-nm excimer ArF LA system coupled with an Agilent 7500a quadrupole-based ICP-MS (Q-ICP-MS). The detailed analytical procedures are reported in Tang et al. (2021). During LA, a National Institute of Standards and Technology (NIST) 610 SEM reference material glass was used to optimize the instrumental parameters. Using OD 306 as an external standard, the QH apatite standard (~150 Ma, Chew et al., 2016) was used to verify the analytical accuracy and return the weighted mean $^{206}Pb/^{238}U$ age of 153.3 ± 9.1. In each routine analysis, every 15 sample analyses were followed by twice SRM 610 and OD 306 and once DURANGO and QH, with a repetition of 10 Hz, a laser energy density of 3 J/cm^2, and a spot size of 60 μm. Each spot analysis consists of approximately 30 s background acquisition, 60 s sample data acquisition, and up to 60 s gas blank for flashing sample. The fractionation correction and U–Pb ages were calculated using GLITTER 4.0 (GEMOC, Macquarie University). The Concordia and weighted mean U–Pb age were calculated using the ISOPLOT/EX 4.15 software package.

4.3. Cassiterite U–Pb dating and trace element

Cassiterite LA-ICP-MS U–Pb dating and trace element analyses were conducted at the LA laboratory of the SKLODG, IGCAS. The analytical system comprises a GeoLas Pro 193-nm ArF excimer LA system and an Agilent 7500x ICP-MS instrument. Helium was used as a carrier gas and was mixed with argon via a *T*-connector before entering the ICP-MS. Cassiterite trace element and U–Pb dating analyses were conducted separately, with a repetition of 7 Hz, a laser energy density of 8 J/cm^2, and a spot size of 60 μm. The cassiterite standard was AY–4 (the recommended isotope dilution (ID) thermal ionization (TI) MS age of 158 ± 0.4 Ma, Yuan et al., 2008). It was used as an external standard for cassiterite U–Pb dating and returned the weighted mean $^{206}Pb/^{238}U$ age of 153 ± 2.7 Ma. NIST 612 was used for cassiterite trace element calculation using Sn as the internal standard. The analysis process is reported in more detail by Zhang et al., 2017. The U–Pb age was calculated using the ISOPLOT/EX 4.15 software package.

4.4. Cgms U–Pb dating

CGMs U–Pb isotopic analyses were performed at the SKLODG, IGCAS using a GeoLas Pro 193-nm excimer ArF LS system coupled with an Agilent 7500a Q-ICP-MS. The detailed analysis process was similar to that of Che et al. (2015). To monitor the stability of the instrument and to ensure the reliability of the measured results the zircon standards (91500 and GJ-1) and the coltan standards (Coltan 139) were measured thrice for every fifteen sample points, and the NIST SRM 610 were measured twice for every fifteen sample points. In this study, $^{207}Pb/^{206}Pb$, $^{206}Pb/^{238}U$, $^{207}U/^{205}U$ ($^{235}U=^{238}U/137.88$) and $^{208}Pb/^{232}Th$ rations were corrected using the Coltan 139 as the external standard. All the measured isotope ratios of Coltan 139 during the process of sample analysis were regressed and corrected using reference values for Coltan 139 were set at 2 % (Che et al., 2015). Each spot analysis consists of approximately 30 s background acquisition, 60 s sample data acquisition, and up to 60 s gas blank for flashing sample. The fractionation correction and U–Pb ages were calculated using GLITTER 4.0 (GEMOC, Macquarie University), and the Concordia and weighted mean U–Pb ages were calculated using the ISOPLOT/EX 4.15 software package.

5. Results

5.1. Apatite

As shown in Fig. 4a-c, apatite was commonly 100 to 300 μm in length, with elongation (length-to-width) ratios of 1:1 to 3:1, and no bands or other phenomena were found in any samples collected from the five zones in pegmatite.

The apatite U–Pb dating element composition range are listed in the Table 2 and detailed in the Appendix. Sample A6283 was collected from zone I, and 17 spots were analyzed on this group's grains. The analytical spots gave a Tera–Wasserburg U–Pb lower intercept age of 216.2 ± 9.1 Ma (2σ, n = 17, mean squared weighted deviation (MSWD) = 0.41) (Fig. 5a).

Samples A6286 and A6290 were collected from zone II. The analytical spots gave a Tera–Wasserburg U–Pb lower intercept age of 152.6 ± 9.8 Ma (2σ, n = 36, MSWD = 1.4) (Fig. 6a).

Sample A6298 was collected from zone III, and 22 spots were analyzed on this group's grains. The analytical spots gave a Tera–Wasserburg U–Pb lower intercept age of 201 ± 12 Ma (2σ, n = 22, MSWD = 0.82) (Fig. 7a).

Sample A6302 was collected from zone IV, and 12 spots were analyzed on this group's grains. The analytical spots gave a Tera–Wasserburg U–Pb lower intercept age of 159.1 ± 8.3 Ma (2σ, n = 12, MSWD = 0.70) (Fig. 8a).

Sample A6305 was collected from the zone V, and 20 spots were

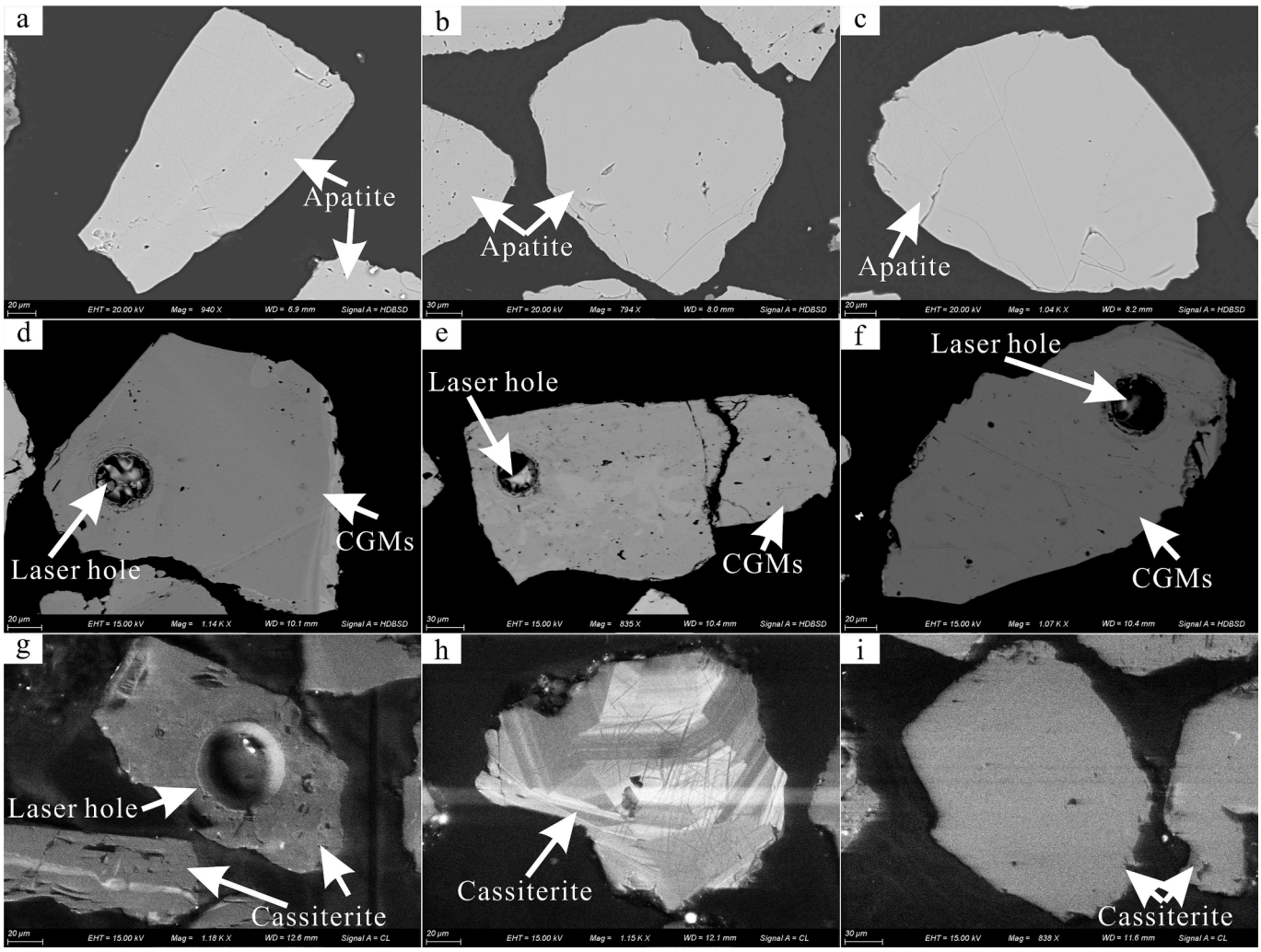

Fig. 4. Representative electron backscattered diffraction (BSE) images of apatite and CGMs and cathodoluminescence (CL) images of cassiterite. (a, b, and c) apatite BSE; (d, e, and f) CGMs BSE; (g, h, and i) cassiterite CL.

Table 2
The U–Pb element composition range of apatite, cassiterite, and CGMs.

Mineral	Location	Sample	Th (ppm)	U (ppm)	Th/U
Apatite	**Zone** I	A6283	2.32–58.2	19.9–1428	0.03–0.19
	Zone II	A6286 and A6290	0.002–116	3.35–697	0.008–2.33
	Zone III	A6298	0.007–41.6	14.1–458	0.002–0.36
	Zone IV	A6302	0.03–52.4	10–233	0.002–0.34
	Zone V	A6305	0.003–0.91	4.35–135	0.0002–0.02
Cassiterite	**Zone** I	A6284	<bld–0.05	0.89–2.99	–
	Zone II	A6287 and A6291	<bld–0.39	0.29–23.8	–
	Zone III	A6295 and A6299	<bld–0.09	1.39–6	–
	Zone IV	A6303	<bld–0.1	1.79–8.14	–
	Zone V	A6306	<bld–0.03	0.94–2.33	–
CGMs	**Zone** II	A6285	0.12–0.8	46.8–227	0.001–0.005
	Zone III	A6293 and A6297	0.05–0.3	77–658	0.0003–0.001
	Zone IV	A6301	0.08–0.67	85–233	0.0004–0.004
	Zone V	A6304	0.09–0.18	31–207	0.0004–0.001

analyzed on this group's grains. The analytical spots gave a Tera–Wasserburg U–Pb lower intercept age of 157.5 ± 6.3 Ma (2σ, n = 20, MSWD = 0.93) (Fig. 8b).

5.2. Cassiterite

In hand samples, cassiterite from the Nanping No.31 pegmatite typically shows euhedral crystal shapes of up to 1 mm. The analyzed cassiterite samples collected from five zones can be divided into two types according to age. Cass-1 comes from zones I, III, IV, and V, and their U–Pb ages are 380 ± 20 Ma. Cass-2 only from zone II, and the U–Pb age is 149.4 ± 6.4 Ma. The CL image of Cass-1 is homogeneous and gloomy (Fig. 4g and i), whereas that of Cass-2 is typically bright with clear and thin oscillatory parallel zones (Fig. 4h).

The cassiterite U–Pb dating element ranges are listed in Table 2, and major and trace element composition data are detailed in the Appendix. Several trace elements show significant differences between cassiterite from zone II and the others, such as Fe, Mn, Nb, Ta, Zr, and Hf (Fig. 9). Furthermore, some trace elements in cassiterite from the Nanping No.31 pegmatite vein are moderately high, such as Al (10.5–2762 ppm), Si (151–9260 ppm), and Ti (34.8–1846 ppm). The concentrations of other trace elements are very low (e.g., ≤13 ppm Li, ≤11 ppm Ga, ≤2 ppm Ge, and ≤ 1 ppm Sr). Sample A6284 was collected from zone I. The analytical spots gave a Tera–Wasserburg U–Pb lower intercept age of 350 ± 14 Ma (2σ, n = 22, MSWD = 0.85) (Fig. 5b).

Samples A6287 and A6291 were collected from zone II. The

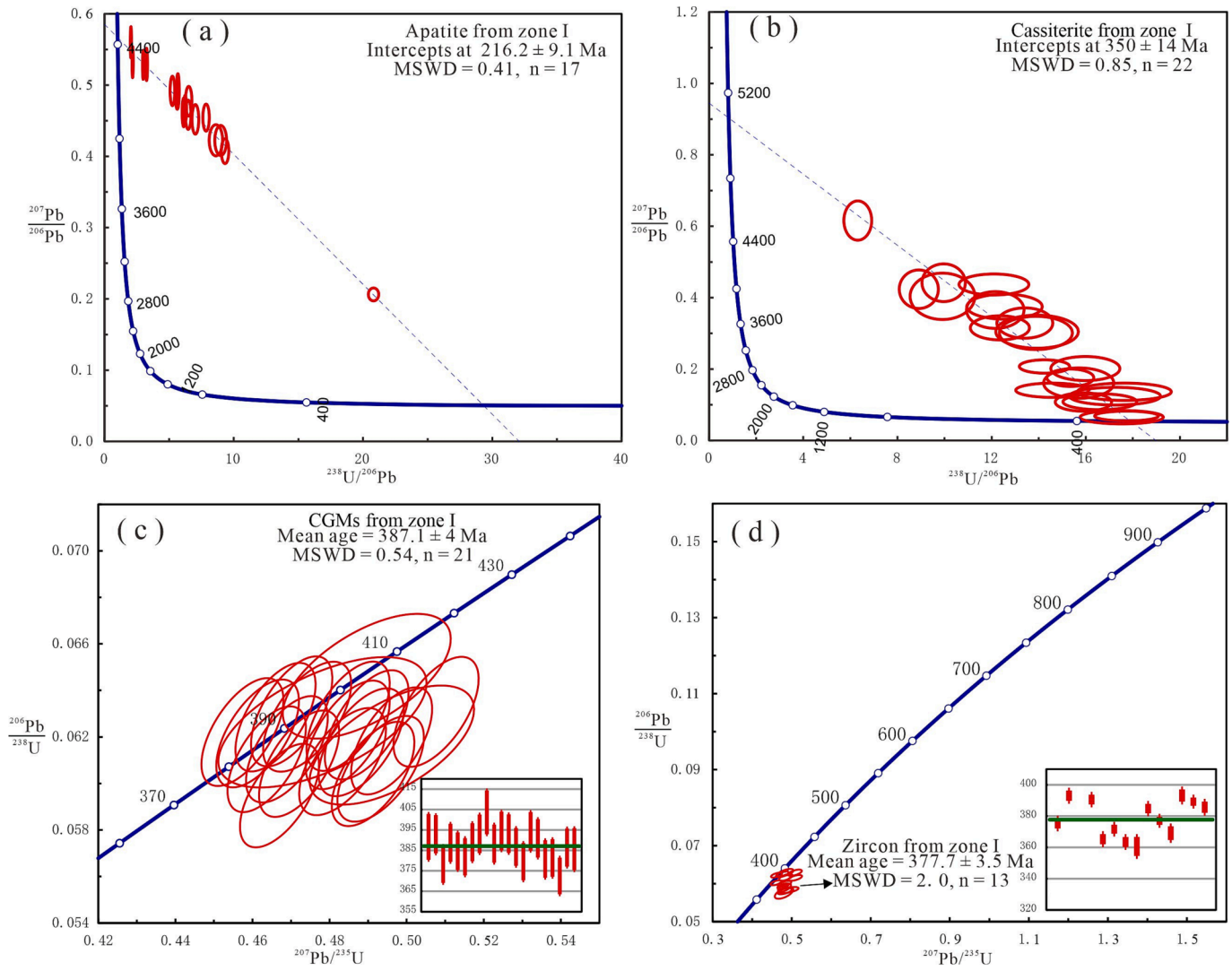

Fig. 5. U–Pb age of the different minerals from zone I in the Nanping No.31 pegmatite. Lower intercept $^{206}Pb/^{238}U$ ages of (a) apatite and (b) cassiterite in the Tera–Wasserburg diagrams. U–Pb Concordia and weighted average diagrams for (c) CGMs (the date from Tang et al., 2017) and (d) zircon (the date from Cai., 2017).

analytical spots gave a Tera–Wasserburg U–Pb lower intercept age of 149.4 ± 6.4 Ma (2σ, n = 38, MSWD = 1.4) (Fig. 6b).

Samples A6295 and A6299 were collected from zone III. The analytical spots gave a Tera–Wasserburg U–Pb lower intercept age of 375 ± 11 Ma (2σ, n = 53, MSWD = 1.3) (Fig. 7b).

Sample A6303 was collected from zone IV. The analytical spots gave a Tera–Wasserburg U–Pb lower intercept age of 380 ± 11 Ma (2σ, n = 25, MSWD = 1.14) (Fig. 8c).

Sample A6306 was collected from zone V. The analytical spots gave a Tera–Wasserburg U–Pb lower intercept age of 379 ± 22 Ma (2σ, n = 14, MSWD = 1.11) (Fig. 8d).

5.3. Cgms

The BSE images show weak compositional zoning in the grains (Fig. 4d), the bright phase is enriched in U and Ti according to EDS analysis, and the cracks are slightly developed (Fig. 4e). Fifty-eight spot analyses on four zoned CGMs show a Ta and Mn increasing trend from zones III, IV, and V to zone II (Fig. 11). According to the element composition, the CGMs samples from zone II are tantalite-(Fe,Mn), from zone III and V are almost columbite-(Fe), and from zone IV are columbite-(Fe), tantalite-(Mn) and two spots are fall into the zone of miscibility gap (Fig. 11). The CGMs U–Pb dating element range are listed in Table 2, and detailed in the Appendix.

Sample A6285 was collected from zone II. The analytical cluster is a tight, coherent group on the Concordia curve, yielding a weighted mean $^{206}Pb/^{238}U$ age of 387 ± 11 Ma (Fig. 6c).

Samples A6293 and A6297 were collected from zone III. The analytical cluster is a tight, coherent group on the Concordia curve, yielding a weighted mean $^{206}Pb/^{238}U$ age of 382.3 ± 6.7 Ma (Fig. 7c).

Samples A6301 and A6304 were collected from zones IV and V, respectively. Nine spot analyses of the CGMs samples from zone IV show a weighted mean $^{206}Pb/^{238}U$ age of 383.1 ± 11 Ma (Fig. 8e), and those from zone V show a weighted mean $^{206}Pb/^{238}U$ age of 370 ± 4.2 Ma (Fig. 8f).

6. Discussion

6.1. Dating different minerals in pegmatite

The zircon U–Pb isotope system is the most widely used in pegmatite dating (Ren et al., 2011; Zhou et al., 2015; Ma et al., 2015; Tang et al., 2017; Lv et al., 2012, 2018a, 2018b, 2021a). Tang et al. (2017) determined the Nanping No. 31 pegmatite vein emplacement age of approximately 387 Ma by U–Pb dating of zircon and CGMs in the zone I (Fig. 5c and d). However, Cai (2017) obtained significantly younger ages

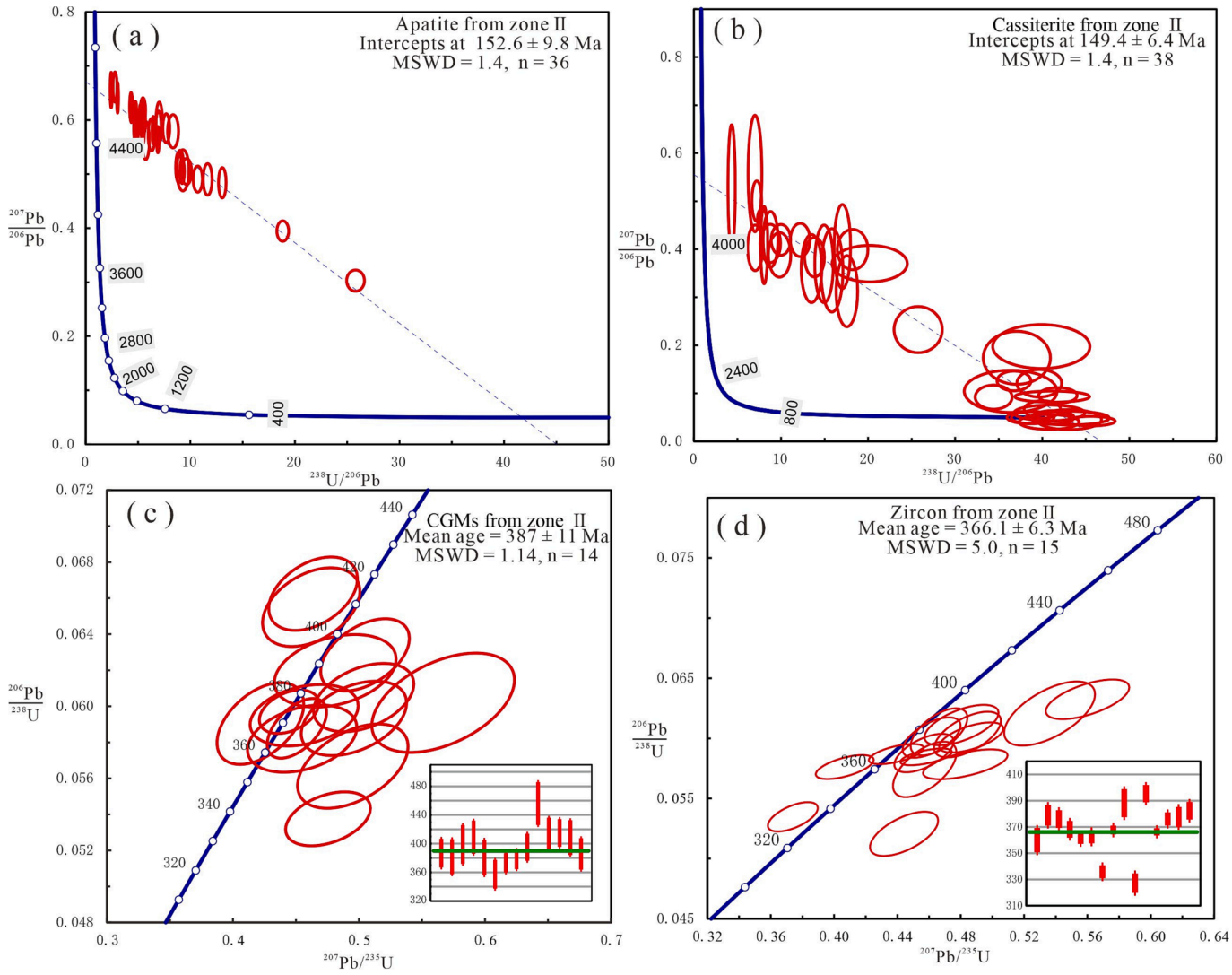

Fig. 6. U–Pb age of the different minerals from zone II in the Nanping No.31 pegmatite. Lower intercept $^{206}Pb/^{238}U$ age of (a) apatite and (b) cassiterite in the Tera–Wasserburg diagram. U–Pb Concordia and weighted average diagrams for (c) CGMs and (d) zircon (the date from Cai., 2017).

when he dating the zircons from zone II and III in Nanping No.31 pegmatite vein (Fig. 6d and Fig. 7d). One of the significant reasons for this result is that the zircon formed in the core zone or highly-fractionated pegmatites are commonly rich in Th and U, which might lead to the metamictization of zircon by radiation damage. It results in a loss of radioactive Pb and misinterpretation of the dating results (Wu and Zheng, 2004). Thus, it is necessary to comprehensively utilize different minerals to evaluate the emplacement age of pegmatites. We discuss the application, limitation, and accuracy of U–Pb dating of apatite, cassiterite and CGMs in pegmatite as follows:

6.1.1. Apatite

Apatite U–Pb dating has been successfully applied in some pegmatites, e.g., Dwight et al. (2016) reported that the LA-ICP-MS U–Pb age of apatite (267.6 ± 7.9 Ma) is consistent with the $^{40}Ar/^{39}Ar$ plateau age of muscovite (253 ± 2.2 Ma) in the pegmatites of the Oxford district of Maine. However, the U–Pb apatite age determinations are limited because of low U and Pb concentrations and high $Pb_{common}/Pb_{radiogenic}$ ratios (Chew et al., 2011), and the age of $^{207}Pb/^{235}U$ vs $^{206}Pb/^{238}U$ typically have a low concordance rate. For the low concordance rate data, it is suggested using the Pb_{common}-unanchored Tera–Wasserburg Concordia Discordia intercept ages to reduce the interference of Pb_{common} and avoid the error caused by deducting Pb_{common} (Chew et al., 2011). The upper intercept represents the age of earth but it is meaningless because of huge errors, and the lower intercept represents the crystallization ages (Tera and Wasserburg, 1972). Thus, the precision of apatite age requires several analyses of a suite of cogenetic apatite grains with a uniformity spread in ^{207}Pb vs ^{206}Pb ratios to define a well-constrained linear array on the Tera–Wasserburg diagram. But the analysis spots of apatite in zones I and III are all near the upper intercept, only one and none spot in the diagrams respectively, failing to constrain the lower intercept (Fig. 5a and Fig. 7a). Therefore, the lower intercept age of apatite from zones I and III have errors. Considering the dating results of other minerals from the same zone, the apatite ages of zones I and III are meaningless (216.2 ± 9.1 Ma and 201 ± 12 Ma, respectively), even if they have seemingly reliable MSWD (MSWD = 0.41 and 0.82, respectively).

Furthermore, due to the low closure temperature (380 °C to 600 °C; Chamberlain and Bowring, 2000; Cherniak and Watson, 2000; Krogstad and Walker, 1994), the chronological data may be younger and record the ages of the latest tectonic thermal event whose temperature exceeds the closure temperature of apatite or the age when the host system cooling to the closure temperature. The cooling rate of pegmatite is controversial, which spans from decades to millions of years (Lv et al., 2018a; London, 2008; 2018). On the one hand, it is assumed the Nanping pegmatite has a long and slow cooling process, and the

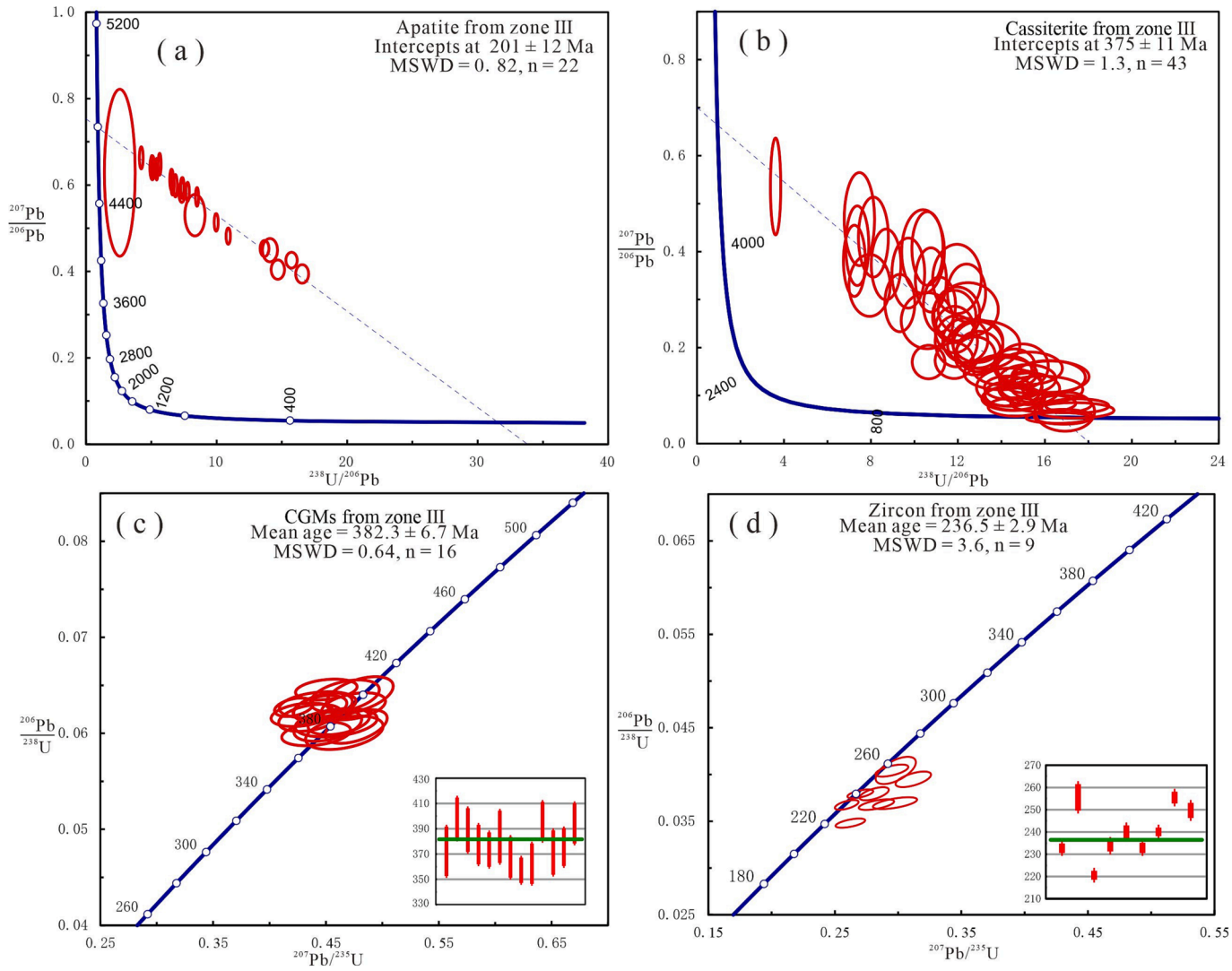

Fig. 7. U–Pb age of the different minerals from zone III in the Nanping No.31 pegmatite. Lower intercept $^{206}Pb/^{238}U$ age of (a) apatite and (b) cassiterite in the Tera–Wasserburg diagram. U–Pb Concordia and weighted average diagrams for (c) CGMs and (d) zircon (the date from Cai., 2017).

pegmatite temperature drops to the closure temperature of apatite U-Pb system at 150 Ma. The conventional closed system may not be able to maintain such a long span, which requires a "heat source" to supply the temperature of pegmatite. Mineralogical and geochemical characteristics suggest that Nanping No.31 pegmatite has multiple stages of evolution after magmatic emplacement (Yang et al., 2003). According to the host stratum estimation, the youngest host stratum of pegmatite is the Neoproterozoic Dikou Formation. It consists predominantly of fine-grained amphibolite facies garnet and sillimanite-bearing biotite gneiss, schist and quartzite. The period of metamorphism and deformation of this stratum is much earlier than pegmatite emplacement (about 600 Ma, Wan et al., 2006). And the emplacing depth of pegmatite is 4.9 Km (Cai, 2017), which is impossible to maintain the temperature of pegmatite for such a long time. From Carboniferous to Jurassic, there is no evidence of the existence of heat source for pegmatite to maintain temperature (such as regional metamorphism or plume). Therefore, we consider that there is no condition for the cooling process of Nanping pegmatite to last 220 Ma. On the other hand, if the Nanping pegmatite cools in a relatively short time after emplacement and is in a relatively low temperature host rock, the significant young age suggests that apatite U-Pb system was reset by later geological process. The northeast of Cathaysian Block experienced the strongest orogeny in the Yanshanian period (150–110 Ma; Zhou et al., 2006; Li et al., 2014), consistent with the dating results of apatite in zones II, IV, and V of the Nanping No.31 pegmatite vein (approximately 150 ± 10 Ma). Besides, based on the investigation of burial and uplift in northeast of the Cathaysian Block, all the zircon fission track ages (ZFT) are about 100 Ma, and the apatite fission track age (AFT) is 20–40 Ma (Zhao et al., 2007; Zhang et al., 2012; Shen et al., 2015; Kang et al., 2017; Yang et al., 2017; Wang et al., 2022). Considering the closure temperature of above methods (apatite U-Pb: 380–600 ℃; ZFT: 140–260 ℃; AFT: 70–150 ℃; Huntington and Klepeis, 2018), it is inferred that Nanping pegmatites experienced a continuous uplift after the peak temperature disturbance of 150 Ma, and uplift to the near surface at 20–40 Ma. Thus, the comprehensive evaluation of the dating results of apatite in zone II, IV, and V indicates that the Nanping No.31 pegmatite vein was affected by the Yanshanian orogeny and suffered severe thermal disturbances at 145–160 Ma (Fig. 12). Therefore, the dating results of apatite in pegmatite should be treated with more caution because the apatite may only date simple postcrystallization histories (rapid thermal relaxation following magmatic emplacement) (Chew et al., 2011). In other words, the apatite U–Pb dating in pegmatite would apply to pegmatite emplaced in the youngest stratum or without suffering tectonic movement.

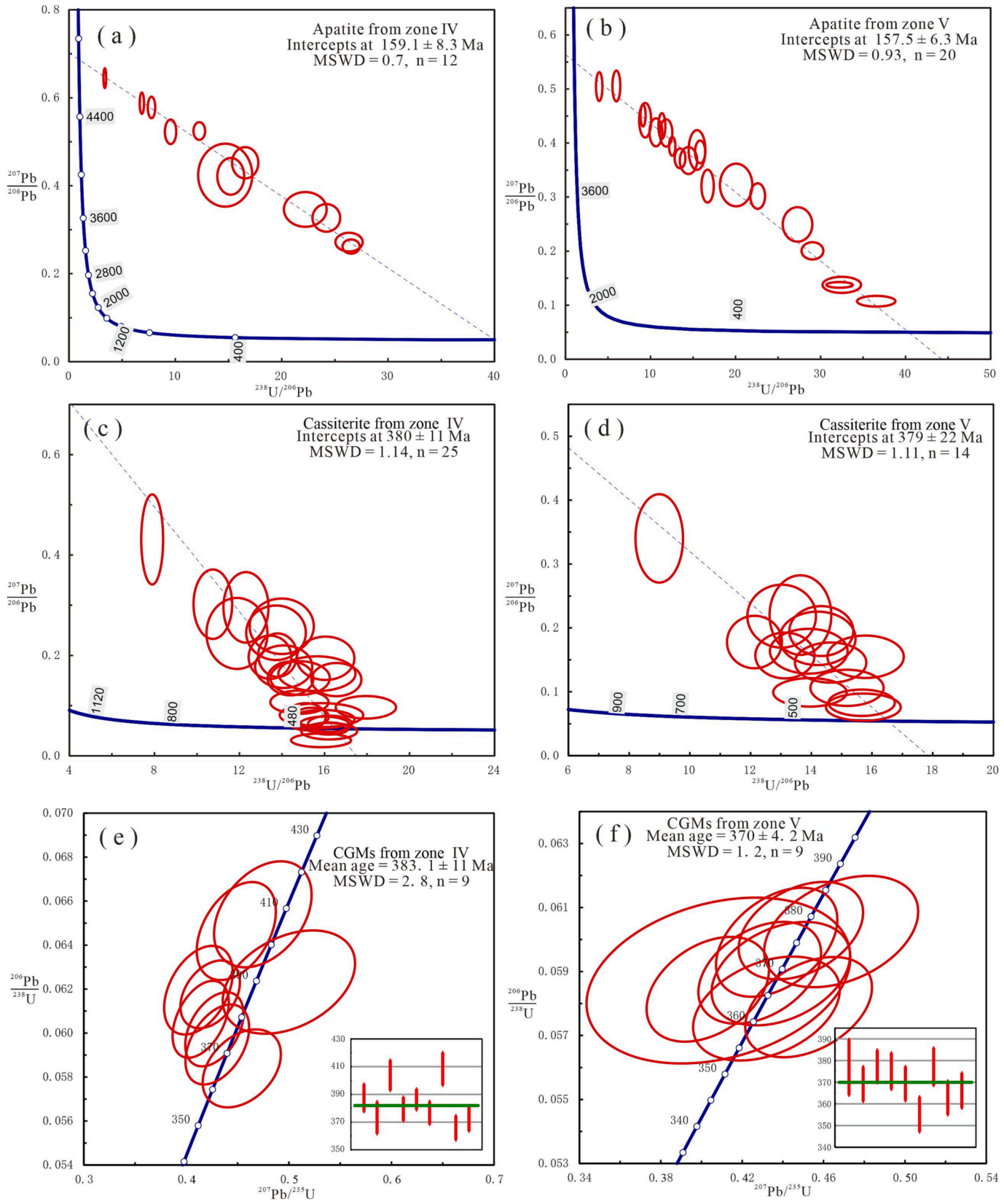

Fig. 8. U–Pb age of the different minerals from zones IV and V in the Nanping No.31 pegmatite. Lower intercept $^{206}Pb/^{238}U$ age of apatite from (a) zone IV and (b) zone V in the Tera–Wasserburg diagram. Lower intercept $^{206}Pb/^{238}U$ age of cassiterite from (c) zone IV and (d) zone V in the Tera–Wasserburg diagram. U–Pb Concordia and weighted average diagrams for CGMs from (e) zone IV and (f) zone V.

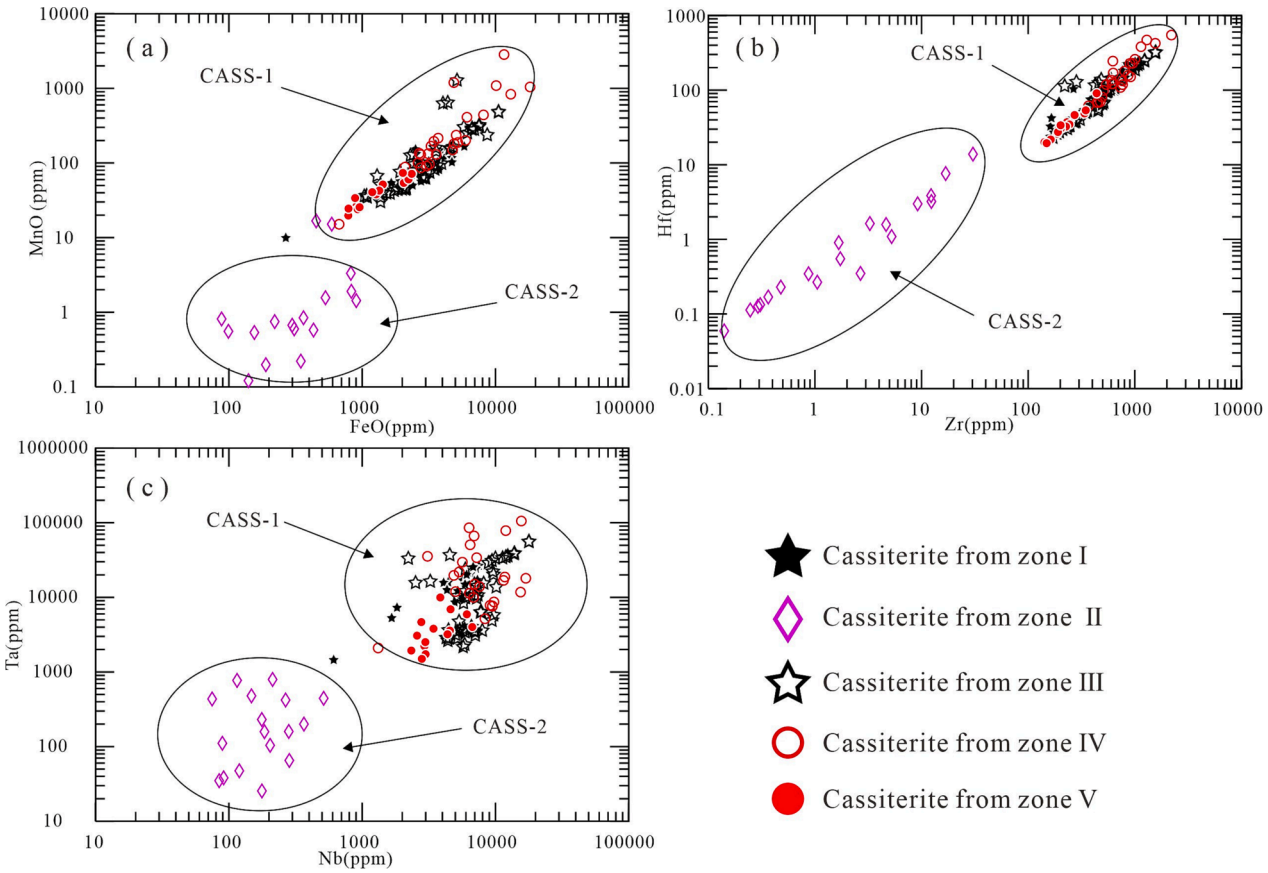

Fig. 9. Binary plots Mn/(Mn + Fe) vs Ta/(Ta + Nb) in the CGMs samples from different zones in the Nanping No.31 pegmatite vein.

6.1.2. Cassiterite

According to the CL characteristics, cassiterites in Nanping No.31 pegmatite vein from five zones are divided into two groups, CASS-1 grains are from zone I, III, IV, V and they are homogeneous (Fig. 4g and i), while CASS-2 grains are from zone II and show internal oscillation band. Studies have shown that the reasons for the internal oscillation band in cassiterite grains are 1) the local fluctuations of hydrothermal fluid composition near the growing crystal surface; 2) variations of available lattice sites on different crystal faces during crystal growth in hydrothermal fluid; and 3) progressive changes in bulk fluid composition during magmatic–hydrothermal evolution (Farmer et al., 1991; Wei et al., 2020). Al and Ti are the luminescence activators, but Fe quenches the luminescence of cassiterite (Remond, 1973; Farmer et al., 1991), consistent with the trace element composition characteristics of cassiterite from the Nanping No.31 pegmatite (Fig. 9). Furthermore, positive correlations among most analyzed elements (Fig. 9) indicate that these elements were incorporated kinetically under high crystallization rates rather than by equilibrium incorporation during cassiterite growth (Rusk, 2012; Mao et al., 2017). The crystal feature of cassiterite is closely related to the crystallization conditions (Dill, 1985). For instance, cassiterite from high-temperature deposits develop stubby prisms with various faces and frequently are twinned; the cassiterite in pegmatite is a common bipyramid crystal without prism (Fig. 10a); medium-temperature (hydrothermal) cassiterite crystals are bipyramidal, with elongated faces of the prism ("needle tin" or "Cornish Type"; Fig. 10b); and the low-temperature hydrothermal cassiterite crystals are fibrous, collomorphous ("wood tin", Fig. 10d, Dill, 2010). Thus, the comparison of CASS-1 (Fig. 10c) and CASS-2 (Fig. 10d) with cassiterite formed various conditions by crystal morphology under microscope suggests that both the CASS-1 and CASS-2 are the crystallized in pegmatitic stage. The crystallization mechanism of zoned pegmatite is controversial (London, 2014; Thomas and Davidson, 2015). Melt immiscibility may be a significant factor (Zhang, 2001; Zhang et al., 2021). If the difference between CASS-1 and CASS-2 is initially formed, suggesting that the temperature is almost unchanged during CASS-1 and CASS-2 crystallization, and the above reasons 1) or 3) may lead to the difference in cassiterite (Farmer et al., 1991; Dill, 1985, 2010; Wei et al., 2020). If the differences caused by later events, suggesting that the later hydrothermal events have transformed the Cass-2.

Cassiterite is a tetragonal rutile mineral, and the ionic radiuses of Pb^{2+} are too large to substitute the octahedrally coordinated tin, whereas the quadrivalent-loving cassiterite prefers the smaller U^{4+} (Yuan et al., 2008; Cheng et al., 2019). Furthermore, cassiterite crystallized in pegmatite typically has a large particle size, meaning that it has moderately high closure temperatures of 450 °C to 780 ℃, closely related to the radius of the grain (Cherniak, 2006). Therefore, cassiterite U–Pb is an accurate method to date the age of pegmatites (Li et al., 2020; Jiang et al., 2021). The Cass-1 and CGMs have the same age, and the emplacement time of pegmatite magma is accurately measured between 370 and 390 Ma (Fig. 12). Combined with the dating results of CGMs from zone II (387 ± 11 Ma, Fig. 6c), it can be inferred that zone II crystallized simultaneously with other zones. However, the age of Cass-2 (149.4 ± 6.4 Ma, Fig. 6b) is coupled with most apatite dating results (150 ± 10 Ma, Fig. 12). Furthermore, the analysis spots of cassiterite from zone II projected on the Tera–Wasserburg diagram are evenly distributed, meaning that the data are reliable. Considering the distinctive CL image, trace element composition, and U–Pb dating results of the CASS-2, if there is the same hydrothermal event to cause the oscillation band and reset the U-Pb age of CASS-2, we infer that zone II may be most severely affected by thermal disturbance than other zones when the Nanping No.31 pegmatite suffered the Yanshanian orogeny. During this period, the closure temperature of CASS-2 was exceeded, resetting the U–Pb closed system and changing the trace element

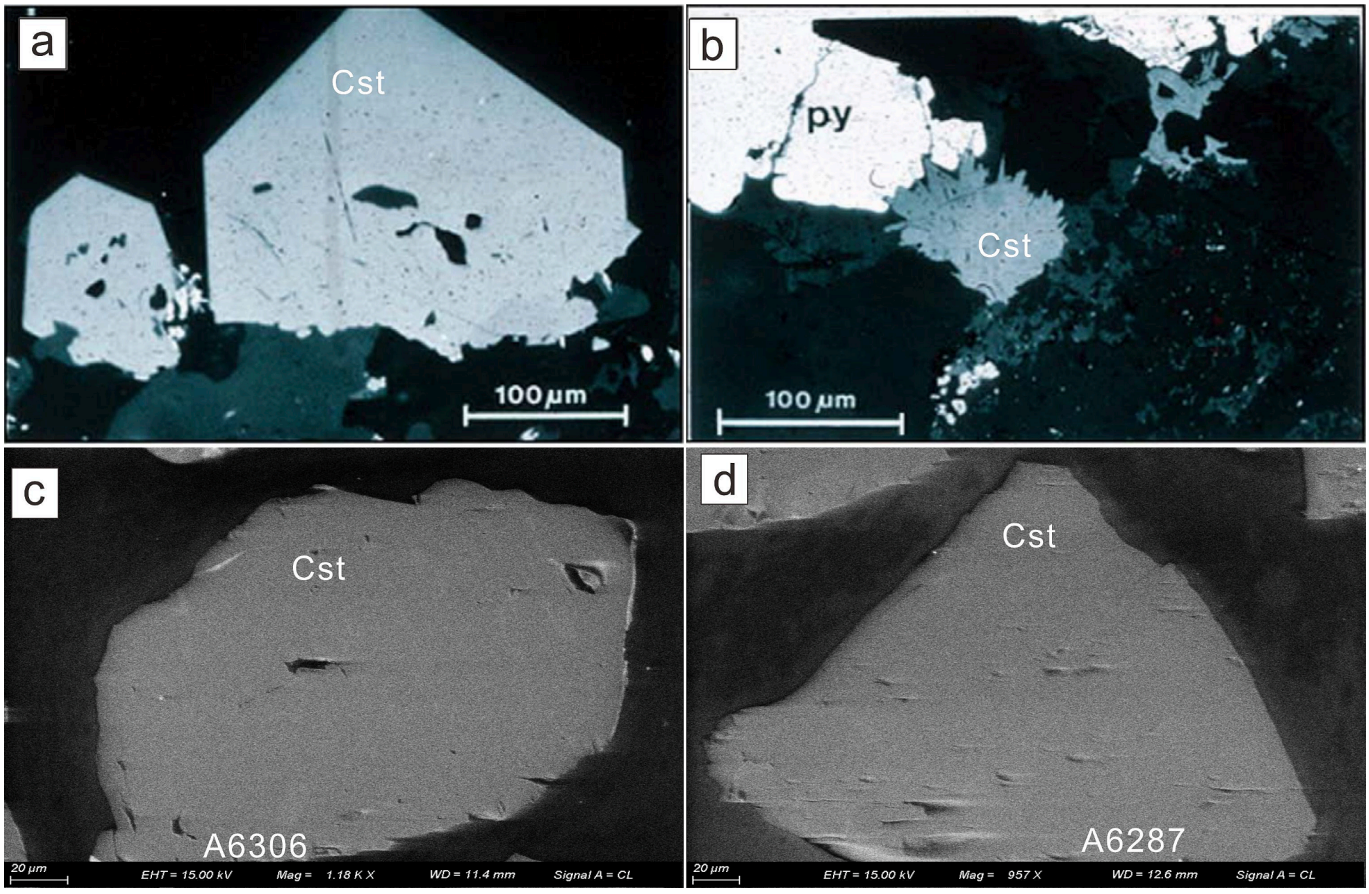

Fig. 10. Crystal morphology of cassiterite (under the microscope). (a) Bipyramidal, stubby crystals of cassiterite from South Crofty, Great Britain (Dill, 2010). (b) Acicular crystals of cassiterite from Kemlas, Germany (Dill, 2010). (c) Stubby crystals of cassiterite from CASS-1. (d) stubby crystals of cassiterite from CASS-2. Cst: cassiterite; Py: pyrite.

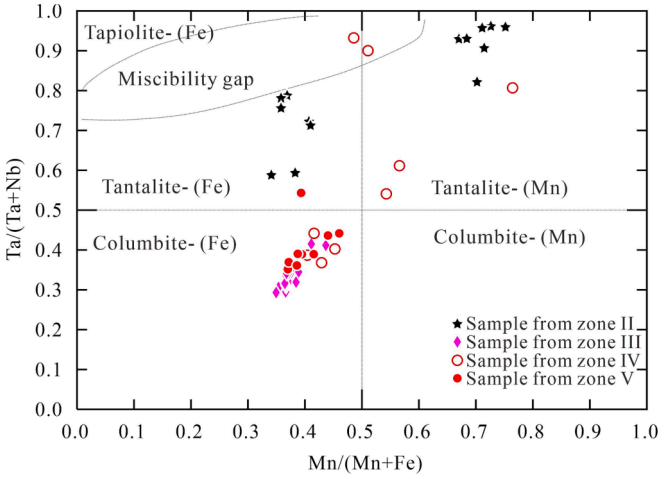

Fig. 11. Binary plots (a) FeO vs MnO, (b) Zr vs Hf, (c) Nb vs Ta in the cassiterite samples from different zones in the Nanping No.31 pegmatite vein.

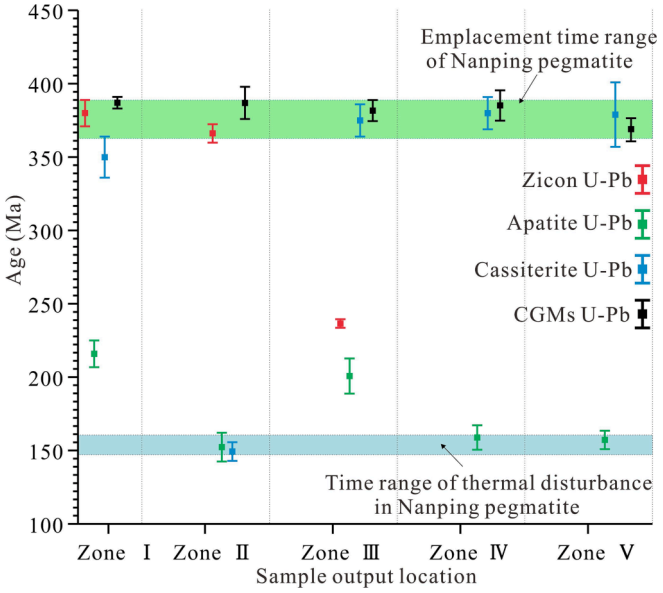

Fig. 12. Box binary diagram showing dating results of different minerals in various zones (zircon data from Cai., 2017 and Tang et al., 2017; the CGMs data in zone I from Tang et al., 2017).

compositions. Furthermore, the oscillation band in the cassiterite grains might have formed in this period, different from previous studies (Farmer et al., 1991; Wei et al., 2020). The thermal disturbance and hydrothermal fluid might induce recrystallization in the cassiterite grains, forming the oscillation band. However, there is no actual evidence to prove the different element content and oscillation band of CASS-2 are coupled with the same event which reset its U-Pb age. The impact of Indosinian orogeny on the northeastern Cathaysian Block is controversial (Zhou et al., 2006; Li and Li, 2007; Li et al., 2012), in addition to the intrusion of S-type granites without contemporaneous volcanism or basic magmatism occur, the thermal history in this period

cannot be evaluated. The magmatic intrusion of Mesozoic S-type granite (such as Jinlong granite, 220 Ma, Fig. 2) was reported that it has no impression on pegmatite (Cai, 2017). Thus, the possibility that other geological processes at the period causing the different element content and oscillation band of CASS-2 cannot be excluded.

In conclusion, although cassiterite is a reliable tool in pegmatite dating, some deficiencies exist, such as that the cassiterite U–Pb system might be reset under severe geological processes. Thus, we propose that after detailed mineralogy and trace element analysis and comparison, the dating results obtained by selecting unaltered cassiterite could more accurately limit the emplacement time of pegmatite.

6.1.3. Cgms

A matrix effect occurs due to the different zircon element compositions (Black et al., 2004), and the U–Pb dating of CGMs using SIMS demonstrates major matrix effects that primarily depend on the Nb/Ta ratio of the CGMs (Legros et al., 2019). However, Che et al. (2015) reported no significant matrix effects in the U–Pb dating of CGMs of different chemical compositions using LA-MC-ICP-MS and Coltan 139 as standards. CGMs samples from all zones in Nanping No.31 pegmatite vein have different major and trace element compositions (Fig. 11). Yang (2003) investigated the CGMs mineralogical characteristics of Nanping No.31 pegmatite vein in detail, and proposed that some grains of CGMs were affected by the later metasomatism stage. However, it seems not affect the CGMs U-Pb age. Because the variations in Nb–Ta and Fe–Mn strongly reflect the extent of fractionation of the columbite–tantalite-bearing pegmatite, there is no correlation between the pegmatite category and age quality, i.e., the columbite–tantalite samples might render closely constrained ages, independent of the overall type or internal zone of the parent pegmatite (Romer and Smeds, 1996). Therefore, the samples of CGMs we analyzed have different major element compositions (Fig. 11), but a consistent age can be obtained. Furthermore, like the zircon, the CGMs would suffer radiation damage when the U content was very high, but it not affects the dating result (even if U content up to 8000 ppm; Feng et al., 2020).

Since Aldrich et al (1956) attempted U–Pb dating of CGMs, the ID-TIMS (Romer and Smeds, 1994, 1996, 1997) and LA-MC-ICP-MS (Smith et al., 2004; Che et al., 2015 and references therein) have been established, developed, and applied to date the age of CGMs from various deposits, and many reliable results have been obtained (Melleton et al., 2012; Camacho et al., 2012; Zhou et al., 2021). These results indicate that LA-MC-ICP-MS is a suitable method for dating CGMs, with < 5 % error in calculated U–Pb ratios (Che et al., 2015; Legros et al., 2019). Unlike the ID-TIMS, the LA-MC-ICP-MS can avoid the influence of uranium mineral inclusions on the dating results. Besides, the closure temperature of the CGMs U–Pb system (700 °C to 620 °C, lower amphibolite facies; Romer and Smeds, 1994) is higher than that of cassiterite and lower zircon and monazite U–Pb. Che et al (2015) investigated the CGMs of the Nanping No.31 pegmatite and obtained an age of 391 ± 4 Ma ($n = 20$) during the pioneering work on CGMs LA-MC-ICP-MS U–Pb dating. Although no evidence existed to verify the reliability at that time, they still proposed that this represented the emplacement age of pegmatite. The dating results of most zircon, cassiterite, and all CGMs in our data (Fig. 12) prove the correctness of his conjecture. CASS-2 and apatite U–Pb ages were reset at 150 ± 10 Ma because of severe thermal disturbances. The CGMs gave reliable pegmatite crystallization and metallogenic age (Fig. 6c), indicating that the Nanping No.31 pegmatite vein was formed over a single magmatic injection. Notably, although most CGMs have low common Pb contents and develop highly radiogenic Pb isotopic compositions with time, the CGMs samples might occasionally have high common Pb concentrations (Che et al., 2019), causing a Disconcordance age of $^{207}Pb/^{235}U$ vs $^{206}Pb/^{238}U$. Scholars typically use a Tera–Wasserburg diagram to obtain the intercept ages from uncorrected data, and the impact of this on the dating results must be further evaluated. Furthermore, the ^{207}Pb and ^{206}Pb isotopes are much easier affected by the background and common Pb compositions than ^{238}U. Thus, $^{206}Pb/^{238}U$ ages are recommended (Che et al., 2015; Legros et al., 2019). In conclusion, we propose that CGMs U–Pb dating can provide reliable age constraints in pegmatite.

6.2. The age of different zones in pegmatite

Due to the dating results of the minerals from five zones, it is obvious that in the Nanping No.31 pegmatite vein, the minerals located in the zone II are easily disturbed by later geological processes (Fig. 12), such as the resetting age of apatite and cassiterite, and the zircon also lose lost some radioactive Pb, resulting in younger age. Only the dating results of CGMs indicate that the zone II crystallized simultaneously with other zones rather than the production of later hydrothermal events.

The structural zone dominated by saccharoidal albite is common in the pegmatite, which is developed in the Koktokay No.3 pegmatite (Zhang, 2001), Littler Three mining area of Ramona, San Diego County, California (London, 2008), Nanping No.31 pegmatite vien (Tang et al., 2017), and other pegmatites. It is usually distributed discontinuously in the wall zone of the pegmatite. According to London et al (2008, 2009), the wall zone of zoned pegmatite is dominated by the mechanism of magma undercooling (Magmatic liquidus minus actual crystallization temperature). The apparent crystal nucleation of saccharoidal albite during crystallization should be much higher than that of other potassium feldspar or microcline in the pegmatitic wall zone. It indicates that the undercooling becomes larger during the crystallization of saccharoidal albite. The essence of increasing undercooling is the change of relative temperature. There are two mechanisms to change the relative temperature: 1) change of absolute temperature: the zone of saccharoidal albite crystallized in a relatively low-temperature stage of the evolution of the wall zone. 2) compositional quench: with the crystallization of the magma, the fluxes components (such as B, P, F) are continuously enriched in the residual magma. Experiments show that trace fluxes components can significant change the liquidus temperature of magma (London and George, 2017). Many geological and geochemical evidences indicated that the whole wall zone of pegmatite crystallized in the early stage (e.g., Jahns and Burnham, 1969; Zhang, 2001; Bachmann and Bergantz, 2004; London, 2008, 2009, 2018; London et al., 2019), but there is no evidence that there is a relatively low-temperature stage or obvious temperature change in the crystallization process of wall zone in pegmatite, the crystal characteristics of CASS-2 under the microscope also prove that the temperature of pegmatitic system has no obvious change in the crystallization zone II. Thus, it is reasonable to consider the mechanisms 2) are dominate in the crystallization process of saccharoidal albite. The saccharoidal structure makes the micro fissures in the zone develop, which is conducive to the subsequent fluid migration. Thus, the degree of transformation of minerals in the saccharoidal albite zone is aggravated, even in the same geological event, the minerals in this zone would be more affected.

6.3. Comparison and enlightenment of different dating methods in pegmatite

In summary, different dating methods from different zones in the Nanping No.31 pegmatite rare metals deposit record the time of thermal events in various stages. Most cassiterite, and all CGMs ages record the emplacement age of pegmatitic magma. Whereas apatite from zone II, III, V and cassiterite from zone II reset the U–Pb age due to the Yanshanian orogeny and suffered severe thermal disturbance, therefore, they record the age of thermal events. These results correlate well with those of previous scholars. The zircon U–Pb ages of rare-metal granitic pegmatites are consistent with those of CGMs (Glodny et al., 1998; Camacho et al., 2012; Deng et al., 2013), which can accurately obtain the emplacement age of pegmatite magma. Simultaneously, it proves that most cassiterite U–Pb ages are reliable (Yuan et al., 2011; Kendall-Langley et al., 2020; Fei et al., 2020; Li et al., 2020) and can be used to limit the age of pegmatites. However, the apatite U–Pb age is younger

due to the limitation of closure temperatures and other factors, which must be approached more circumspectly.

Considering the problem of pegmatite dating and the applicability and limitations of various dating methods, the final determination of the emplacement and metallogenic ages of rare metal pegmatite requires comprehensive investigations of different methods to obtain reliable age. Generally, the emplacement depth of pegmatite is relatively shallow. According to thermodynamic simulation (London, 2008), the cooling time span of pegmatitic magma would not be long without additional heat supply. The crystallization of a single pegmatite vein body spans an insignificant time relative to age-dating precision (London, 2008). Thus, we speculate that the cooling time span of mots pegmatite would not be very long, according to the current dating methods, it seems impossible to accurately limit the formation process of pegmatite crystallization using different mineral dating methods from different zones. The errors between single results have reached approximately a million grades, far exceeding the crystallization time of pegmatite. Petrography, mineral assemblage, and isotope characteristics make it more reliable to explore the evolution sequence of the zone of pegmatite. Even Harding and Tanco pegmatites with large-scale and complex zoning have been cooled and crystallized only approximately 1000 years (Chakoumakos and Lumpkin, 1990; London, 2008). Despite multimineral dating methods applied to pegmatite dating, new methods are in continuous development. For instance, the recently developed garnet in situ U–Pb dating is worthy of attempt and application for numerous garnets crystallized in the outer zone of pegmatite (Deng et al., 2017; Tang et al., 2021 Jiang et al., 2021).

7. Conclusions

(1) LA-ICP-MS U–Pb dating of all CGMs, and cassiterite from zones I, III, IV, V in the Nanping No.31 pegmatite vein reveals that the emplacement of the Nanping pegmatites occurred at 370–390 Ma, and Nb–Ta–Sn mineralization are almost simultaneous. LA-ICP-MS U–Pb dating of cassiterite from zone II and apatite from all the zones reveal that the Nanping No.31 pegmatite vein experienced severe thermal disturbances between 145 and 160 Ma, which might be related to orogeny in the Yanshanian period.

(2) The structural zone dominated by saccharoidal albite is usually located in the wall zone of zoned pegmatite. Due to the special formation mechanism, it may be more easily disturbed by later geological processes. Thus, the chronological data from this zone minerals should be approached more cautious.

(3) The dating of rate metal pegmatite deposit has been a problem for a long time, and it is necessary to consider the applicability and limitations of various methods comprehensively. In addition to zircon, the CGMs, cassiterite, apatite, garnets, and other minerals should be used to determine the age accurately.

Declaration of Competing Interest

The authors declare that they have no known competing financial interests or personal relationships that could have appeared to influence the work reported in this paper.

Data availability

Data will be made available on request.

Acknowledgments

This study is jointly supported by the Key Program of the National Natural Science Foundation of China (No. 91962222, No. 41773053 and 42173043) and Guizhou Provincial 2019 Science and Technology Subsidies (No. GZ2019SIG).

Data availability

All data are supplied within the supplementary files.

References

Aldrich, L.T., Davis, G.L., Tilton, G.R., Wetherill, G.W., 1956. Radioactive ages of minerals from the Brown Derby mine and Quartz Creek granite near Gunnison, Colorado. Journal of Geophysical Research: Solid Earth 61 (2), 215–232.

Bachmann, O., Bergantz, G.W., 2004. On the origin of crystal-poor rhyolites extracted from batholithic crystal musher. Journal of Petrology 45, 1565–1582.

Baumgartner, R., Romer, R.L., Moritz, R., Sallet, R., Chiaradia, M., 2006. Columbite–tantalite-bearing granitic pegmatites from the serido belt, Northeastern Brazil: genetic constraints from U-Pb dating and Pb isotopes. The Canadian Mineralogist 44, 69–86.

Black, L.P., Kamo, S.L., Allen, C.M., Davis, D.W., Aleinikoff, J.N., Valley, J.W., Mundil, R., Campbell, I.H., Korsch, R.J., Williams, I.S., Foudoulis, C., 2004. Improved $^{206}Pb/^{238}U$ microprobe geochronology by the monitoring of a trace-element-related matrix effect; SHRIMP, ID-TIMS, ELA-ICP-MS and oxygen isotope documentation for a series of zircon standards. Chemical Geology 205, 115–140.

Cai, D.W., Tang, Y., Zhang, H., Lv, Z.H., Liu, Y.L., 2016. Petrogenesis and tectonic setting of the Devonian Xiqin A-type granite in the northeastern Cathaysia Block, SE China. Journal of Asian Earth Science 141, 43–58. https://doi.org/10.1016/j. jseaes. 2016. 05. 015.

Cai, D.W., 2017. The genetic relationship and tectonic setting of the late Paleozoic Nanping granite and No.31 pegmatite vein in Fujian province. Doctor Thesis. Insitute of Geochemistry, Chinese Academy of Science, 1–90 (in Chinese with English summary).

Camacho, A., Baadsgaard, H., Davis, D.W., Černý, P., 2012. Radiogenic isotope systematics of the Tanco and Silverleaf granitic pegmatites, Winnipeg River pegmatite district. Manitoba. The Canadian Mineralogist 50 (6), 1775–1792.

Chakoumakos, B.C., Lumpkin, G.R., 1990. Pressure-temperature constraints on the crystallization of the Harding pegmatite, Taos County. New Mexico. The Canadian Mineralogist 28 (2), 287–298.

Chamberlain, K.R., Bowring, S.A., 2000. Apatite-feldspar U-Pb thermochronometer: a reliable, mid-range-450°C diffusion-controlled system. Chemical Geology 172, 173–200.

Che, X.D., Wu, F.Y., Wang, R.C., Gerdes, A., Ji, W.Q., Zhao, Z.G., Yang, J.H., Zhu, Z.Y., 2015. In situ U-Pb isotopic dating of columbite–tantalite by LA-ICP-MS. Ore Geology Reviews 65 (4), 979–989.

Che, X.D., Wang, R.C., Wu, F.Y., Zhu, Z.Y., Zhang, W.L., Hu, H., Xie, L., Lu, J.J., Zhang, D., 2019. Episodic Nb-Ta mineralization in South China: Constraints from in situ LA-ICP-MS columbite–tantalite U-Pb dating. Ore Geology Reviews 105, 71–85.

Cheng, Y.B., Spandler, C., Kemp, A., Mao, J.W., Rusk, B., Hu, Y., Blake, K., 2019. Controls on cassiterite (SnO_2) crystallization: Evidence from cathodoluminescence, trace-element chemistry, and geochronology at the Gejiu tin district. American Mineralogist 104, 118–129.

Cherniak, D.J., 2006. Pb and rare earth element diffusion in xenotime. Lithos 88 (1), 1–14.

Cherniak, D.J., Watson, E.B., 2000. Pb diffusion in zircon. Chemical Geology 172, 5–24.

Chew, D.M., Babechuk, M.G., Cogné, N., 2016. LA-Q-ICPMS trace-element analyses of Durango and McClure Mountain apatite and implications for making natural LA-ICPMS mineral standards. Chemical Geology 435, 35–48.

Chew, D.M., Sylvester, P.J., Tubrett, M.N., 2011. U-Pb and Th-Pb dating of apatite by LA-ICPMS. Chemical Geology 280, 200–216.

Deng, X.D., Zhao, X.F., Hu, Z.C., Hu, H., Selby, D., de Souza, Z.S., 2013. U-Pb isotope and trace element analysis of columbite- (Mn) and zircon by laser ablation ICP-MS: Implications for geochronology of pegmatite and associated ore deposits. Chemical Geology 344, 1–11.

Deng, X.D., Li, J.W., Luo, T., Wang, H.Q., 2017. Dating magmatic and hydrothermal processes using andradite-rich garnet U-Pb geochronometry. Contributions to Mineralogy and Petrology 172 (9), 71. https://doi.org/10.1007/s00410-017-1389-2.

Dill, H.G., 1985. Die Vererzung am Westrand der Böh-mischen Masse. Metallogenese in einer ensialischen Oro-genzone. Geol. Jahrb. 73, 3–461.

Dill, H.G., 2010. The "chessboard" classification scheme of minerals deposits: Mineralogy and geology from aluminum to zirconium. Earth-Science Reviews 100, 1–420.

Dill, H.G., 2016. The CMS classification scheme (Chemical composition-Mineral assemblage-Structural geology)-linking geology to mineralogy of pegmatitic and aplitic rocks. Neues Jahrbuch für Mineralogie-Abhandlungen: J. Mineral. Geochem. 193(3), 231–263.

Dill, H.G., 2015. Pegmatites and aplites: Their genetic and applied ore geology. Ore Geology Reviews 69, 417–561.

Dwight, B., Erin, S., Robert, B., Sam, B., Jeff, B., Paul, O.S., Andrew, M., 2016. Geochronology and tectonic context of lithium-cesium-tantalum pegmatites in the Appalachians. The Canadian Mineralogist 54, 945–969.

European Commission., 2020. Critical Raw Materials Resilience: Charting a Path towards greater Security and Sustainability. (https://eur-lex.europa.eu/legal-content/EN/TXT/PDF/?uri=CELEX:52020DC0474&from=EN).

Farmer, C.B., Searl, A., Halls, C., 1991. Cathodoluminescence and growth of cassiterite in the composite lodes at South Crofty mine, Cornwall, England. Mineralogical Magazine 55, 447–458.

Fei, G.C., Yang, Z., Yang, J.Y., Luo, W., Deng, Y., Lai, Y.T., Tao, X.X., Zheng, L., Tang, W. C., Li, J., 2020. New precise timing constraint for the Dangba granitic pegmatite type

rare-metal deposits, Markam, Sichuan Province: Evidence from cassiterite LA-MC-ICP-MS U-Pb dating. Acta Geological Sinica 94 (3), 836–849 in Chinese with English abstract.
Feng, Y.G., Liang, T., Robert, L., Zhang, Z., Zhou, Y., Zhang, Z.L., Gao, J.G., 2020. LA-ICP-MS dating of high-uranium columbite from no.1 pegmatite at Dakalasu, the Chinese Altay orogen: Assessing effect of metamictization on age concordance. Lithos 362–363, 105461 doi: 10.1016/j.lithos.2020.105461.
Geisler, T., Pidgeon, R.T., Bronswijk, W., Kurtz, R., 2002. Transport of uranium, thorium, and lead in metamict zircon under low-temperature hydrothermal conditions. Chemical Geology 191, 141–154.
Geisler, T., Schaltegger, U., Tomaschek, F., 2007. Re-equilibration of zircon in aqueous fluids and melts. Elements 3, 43–50.
Glodny, J., Grauert, B., Fiala, J., Vejnar, Z., Krohe, A., 1998. Metapegmatites in the wester Bohemian massif: Ages of crystallization and metamorphic overprint, as constrained by U-Pb zircon, monazite, garnet, columbite and Rb-Sr muscovite data. Geologische Rundschau 87 (1), 124–134.
Hou, Z.Q., Chen, J., Zhai, M.G., 2020. Current status and frontiers of research on critical mineral resources. Chinese Science Bulletin 65 (33), 3651–3652.
Huntington, K.W., Klepeis, K.A., 2018. Challenges and opportunities for research in tectonics: Understanding deformation and the processes that link Earth systems, from geologic time to human time. A community vision document submitted to the U.S, National Science Foundation.
Jahns, R.H., Burnham, C.W., 1969. Experimental studies of pegmatite genesis: I. A model for the derivation and crystallization of granitic pegmatites. Economic Geology 64 (8), 843–864.
Jiang, S.Y., Wang, C.L., Zhang, L., Yuan, F., Su, H.M., Zhang, H.X., Liu, T., 2021. In situ trace element tracing and isotopic dating of pegmatite type lithium deposits: an overview. Acta Geologica Sinica 95 (10), 3017–3038 in Chinses with English abstract.
Kang, C.X., Zhou, Y., Fan, F.P., Miao, N., Li, F.C., Sun, J.D., et al., 2017. Geochemical characteristic, zircon U-Pb ages, and Lu-Hf isotopic compositions of the Yongfu Pluton in Longyan, Fujian Province. Geotecton. Metallog. 41, 960–973. (In Chinese with English abstract) https://doi. org/10.16539/j.ddgzyckx.2017.05.012.
Kendall-Langley, L.A., Kemp, A.I.D., Grigson, J.L., Hammerli, J., 2020. U-Pb and reconnaissance Lu-Hf isotope analysis of cassiterite and columbite group minerals from Archean Li-Cs-Ta type pegmatites of western Australia. Lithos 352–353, 105231.
Krogstad, E.J., Walker, R.J., 1994. High closure temperatures of the U-Pb system in large apatites from the Tin Mountain pegmatite, Black Hills, South Dakota, USA. Geochemical and Cosmochemical Review 58, 3845–3853.
Legros, H., Mercadier, J., Villeneuve, J., Romer, R.L., Deloule, E., Van Lichtervelde, M., Dewaele, S., Lach, P., Che, X.D., Wang, R.C., Zhu, Z.Y., Gloahuen, E., Melleton, J., 2019. U-Pb isotopic dating of columbite–tantalite minerals: development of reference materials and in situ applications by ion microprobe. Chemical Geology 512, 69–84.
Li, H., Hong, T., Yang, Z.Q., Chen, J.Z., Ke, Q., Wang, X.H., Niu, L., Xu, X.W., 2020. Comparative studying on zircon, cassiterite and CGMs U-Pb dating and 40Ar/39Ar dating of muscovite rare-metal granitic pegmatites: A case study of the northern Tugeman lithium-beryllium deposit in the middle of Altyn Tagh. Acta Petrological Sinica 36 (9), 2869–2892. https://doi.org/10.18654/1000-0569/2020.09.16 in Chinses with English abstract.
Li, X.H., Li, Z.X., Li, W.X., Wang, Y.J., 2006. Initiation of the Indosinian Orogeny in South China: Evidence for a Permian Magmatic Arc on Hainan Island. Journal of Geology 114 (3), 341–353.
Li, Z.X., Li, X.H., 2007. Formation of the 1300-km-wide intracontinental orogen and postorogenic magmatic province in Mesozoic South China: a flat-slab subduction model. Geology 35 (2), 179–182.
Li, X.H., Li, Z.X., He, B., Li, W.X., Li, Q.L., Gao, Y.Y., 2012. The Early Permian active continental margin and crustal growth of the Cathaysia Block: in into U-Pb, Lu–Hf and O isotope analyses of detrital zircons. Chemical Geology 328 (11), 195–207.
Li, X.H., Li, Z.X., Li, W.X., 2014. Detrital zircon U-Pb and Hf isotope constrains on the generation and reworking of Precambrian continental crust in the Cathaysia Block. South China: A synthesis. Gondwana Research 25 (3), 1202–1215.
London, D., 2008. Pegmatites. The Canadian Mineralogist Special Publication 10. The Mineralogical Association of Canada, pp. 10–347.
London, D., 2009. The origin of primary textures in granitic pegmatites. Canadian Mineralogist 47, 697–724.
London, D., 2014. A petrologic assessment of internal zonation in granitic pegmatites. Lithos 184–187, 74–104.
London, D., 2018. Ore-forming processes within granitic pegmatites. Ore Geology Reviews 101, 349–383.
London, D., George, M., 2017. Experimental Crystallization of the Macusani Obsidian, with Applications to Lithium-rich Granitic Pegmatites. Journal of Petrology 1–26.
London, D., Lindsey, E.H., Christine, R.S., Brandon, M.G., 2019. Feldspar thermometry in pegmatites: truth and consequences. Mineralogy and Petrology 175, 8.
Lv, Z.H., Zhang, H., Tang, Y., Guan, S.J., 2012. Petrogenesis and magmatic-hydrothermal evolution time limitation of Kelumute No.112 pegmatite in Altay, Northwestern China: evidence from zircon U-Pb and Hf isotopes. Lithos 154, 374–391.
Lv, Z.H., Zhang, H., Tang, Y., 2018a. Lanthanide tetrads with implications for liquid immiscibility in an evolving magmatic-hydrothermal system: Evidence from rare earth elements in zircon from the No.112 pegmatite, Kelumute, Chinese Altai. Journal of Asian Earth Sciences 164, 9–22.
Lv, Z.H., Zhang, H., Tang, Y., 2018b. Petrogenesis of syn-orogenic rare metal pegmatites in the Chinese Altai: evidences from geology, mineralogy, zircon U-Pb age and Hf isotope. Ore Geology Reviews 95, 161–181.
Lv, Z.H., Zhang, H., Tang, Y., 2021a. Anatexis origin of rare metal/earth pegmatites: Evidences from the Permian pegmatites in the Chinese Altai. Lithos 380–381, 105865.
Lv, Z.H., Chen, J., Zhang, H., Tang, Y., 2021b. Petrogenesis of Neoproterozoic rare metal granite-pegmatite suite in Jiangnan Orogen and its implications for rare metal mineralization of peraluminous rock in South China. Ore Geology Reviews 128, 103923.
Ma, Z.L., Zhang, H., Tang, Y., Lv, Z.H., Zhang, X., Zhao, J.Y., 2015. Zircon U-Pb geochronology and Hf isotopes from the Kaluan mining area in the Altay, Xinjiang and their genetic relationship with the Halong granite. Geochimica 44 (1), 9–26 in Chinese with English abstract.
Mao, W., Rusk, B., Yang, F., Zhang, M., 2017. Physical and chemical evolution of the Dabaoshan porphyry Mo deposit, South China: Insights from fluid inclusions, cathodoluminescence, and trace elements in quartz. Economic Geology 112, 889–918.
McCauley, A., Bradley, D.C., 2014. The global age distribution of granitic pegmatites. The Canadian Mineralogist 52 (2), 183–190.
Melcher, F., Graupner, T., Gäbler, H.E., Sitnikova, M., Friedhelm, H.K., Oberthür, T., Gerdes, A., Dewaele, S., 2015. Tantalum-(niobium-tin) mineralization in African pegmatites and rare metal granites: Constraints from Ta–Nb oxide mineralogy, geochemistry and U-Pb geochronology. Ore Geology Reviews 64, 667–719.
Melleton, J., Gloaguen, E., Frei, D., Novak, M., Breiter, K., 2012. How are the emplacement of rare-element pegmatites, regional metamorphism and magmatism interrelated in the Moldanubian Domain of the Variscan Bohemian Massif, Czech Republic? The Canadian Mineralogist 50 (6), 1751–1773.
Qiu, N.M., Yang, Y.Q., 1985. Nanping Granitic Pegmatite (in Chinese with English abstract).
Remond, G., 1973. Exemples d'identification et de localization des elements en trace dans les mineraux luminescents a l'aide de la microsonde ionique. Bulletin de la Société française de Minéralogie et de Cristallographie 96, 183–198.
Ren, B.Q., Zhang, H., Tang, Y., Lv, Z.H., 2011. LA-ICPMS U-Pb zircon geochronology of the Altai pegmatites and its geological significance. Acta Mineralogica Sinica 31 (3), 587–596 in Chinese with English abstract.
Romer, R.L., Smeds, S.A., 1994. Implications of U-Pb ages of columbite–tantalites from granitic pegmatites for the Palaeoproterozoic accretion of 1.90 –1.85 Ga magmatic arcs to the Baltic Shield. Precambrian Research 67 (1–2), 141–158.
Romer, R.L., Smeds, S.A., 1996. U-Pb columbite ages of pegmatites from Sveconorwegian terranes in southwestern Sweden. Precambrian Research 76 (1–2), 15–30.
Romer, R.L., Smeds, S.A., 1997. U-Pb columbite chronology of post-kinematic Palaeoproterozoic pegmatites in Sweden. Precambrian Research 82 (1–2), 85–99.
Rusk, B.G., 2012. Cathodoluminescent textures and trace elements in hydrothermal quartz. In: Gotze, J., Mockel, R. (Eds.), Quartz: Deposits, Mineralogy and Analytics, 1st ed. Springer Geology, pp. 307–329.
Shen, M.T., Zhou, Y., Zhang, X.D., Wu, B., 2015. LA-ICP-MS U-Pb dating of the zircon from Xikou intrusives in Shanghang Area, Southwetern Fujian, and its geological significance. In Chinese with English Abstract Geol. Rev. 61, 913–924. https://doi.org/10.16509/j. georeview.2015.04.018.
Shu, L.S., Zhou, X.M., Deng, P., Wang, B., Jiang, S.Y., Yu, J.H., Zhao, X.X., 2009. Mesozoic tectonic evolution of the Southeast China Block: new insights from basin analysis. Journal of Asian Earth Sciences 34, 376–391.
Shu, L.S., Wang, B., Cawood, P.A., Santosh, M., Xu, Z.Q., 2015. Early Paleozoic and Early Mesozoic intraplate tectonic and magmatic events in the Cathaysia Block. South China. Tectonics 34 (8), 1600–1621.
Smith, S.R., Foster, G.L., Romer, R.L., Tindle, A.G., Kelley, S.P., Noble, S.R., Horstwood, M., Breaks, F.W., 2004. U-Pb columbite-tantalite chronology of rare-element pegmatites using TIMS and Laser Ablation-Multi Collector-ICP-MS. Contributions to Mineralogy and Petrology 147 (5), 549–564.
Tang, Y.W., Gao, J.F., Lan, T.G., Cui, K., Han, J.J., Zhang, X., Chen, Y.W., Chen, Y.H., 2021. In situ low-U garnet U-Pb dating by LA-SF-ICP-MS and its application in constraining the origin of Anji skarn system combined with Ar–Ar dating and Pb isotopes. Ore Geology Reviews 130, 103970.
Tang, Y., Zhao, J.Y., Zhang, H., Cai, D.W., Lv, Z.H., Liu, Y.L., Zhang, X., 2017. Precise columbite-(Fe) and zircon U-Pb dating of the Nanping No.31 pegmatite vein in northeastern Cathaysia Block. SE China. Ore Geology Reviews 83, 300–311.
Tera, F., Wasserburg, G.J., 1972. U-Th-Pb systematics in three Apollo 14 basalts and the problem of initial Pb in lunar rocks. Earth and Planetary Science Letters 14, 281–304.
Thomas, R., Davidson, P., 2015. Comment on "A petrologic assessment of internal zonation in granitic pegmatites" by David London (2014). Lithos 212–215, 462–468.
Tkachev, A.V., 2011. Evolution of metallogeny of granitic pegmatites associated with orogens throughout geologic time. Granite-Related Ore Deposits. Geological Society of London Special 350, 7–23.
M. Van Lichtervelde A. Grand'Homme M. Saint-Blanquat P. Olivier A. Gerdes J.L. Paquette J.C. Melgarejo E. Druguet P. Alfonso U-Pb geochronology on zircon and columbite-group minerals of the Cap de Creus pegmatites 2017 Miner Petrol NE Spain 10.1007/s00710-016-0455-1.
Wan, Y.S., Liu, D.Y., Xu, M.H., Zhuang, J.M., Song, B., Shi, Y.R., Du, L.L., 2006. SHRIMP U-Pb zircon geochronology and geochemistry of metavolcanic and metasedimentary rocks in Northwestern Fujian, Cathaysia Block, China: Tectonic implications and the need to redefine lithostratigraphic units. Gondwana Research 12, 166–183.
Wang, Y.J., Zhang, A.M., Fan, W.M., Zhang, Y.H., Zhang, Y.Z., 2013. Origin of paleosubduction-modified mantle for Silurian gabbro in the Cathaysia Block: geochronological and geochemical evidence. Lithos 160–161, 37–54.
Wang, Y., Zou, R.G., Cao, K., Xu, X.B., Zattin, M., 2022. Late Mesozoic to Cenozoic exhumation of the SE South China Block: Constraints from zircon and apatite fission-track thermochronology. Tectonophysics 838, 229518.

Wei, M., Zhong, H., Yang, J.H., Tang, Y.W., Liu, L., Fu, Y.Z., Zhang, X.C., Kyaing, S., Soe, M.A., Li, J., Zhang, L., 2020. Combine zircon, Molybdenite, and Cassiterite Geochronology and Cassiterite Geochemistry of the Kuntabin Tin-Tungsten Deposit in Myanmar. Economic Geology 115 (3), 603–625.

Wu, Y.B., Zheng, Y.F., 2004. Genesis of zircon and its constraints on interpretation of U-Pb age. Chinese Science Bulletin 49, 1554–1569.

Yan, Q.H., Qiu, Z.W., Wang, H., Wang, M., Wei, X.P., Li, P., Zhang, R.Q., Li, C.Y., Liu, J. P., 2018. Age of the Dalongliutan rare metal pegmatite deposit, West Kunlun, Xinjiang (NW China): Constraints from LA-ICP-MS U-Pb dating of columbite-(Fe) and cassiterite. Ore Geology Reviews 100, 561–573.

Yang, Y.L., Ni, P., Yan, J., Wu, C.Z., Dai, B.Z., Xu, Y.F., 2017. Early to late Yanshanian I-type granites in Fujian Province, SE China: implications for the tectonic setting and Mo mineralization. J. Asian Earth Sci. 137, 194–219. https://doi.org/10.1016/j.jseaes.2016.11.017.

Yang, Z.M., Song, R.K., Tao, K.J., Zhang, P.S., 2003. Columbite–tantalite minerals from Nanping granitic pegmatites, South China: compositional trends and genetic implications. N. Jb. Miner. Mh. 8, 363–373.

Yuan, S.D., Peng, J.T., Hao, S., Li, H.M., Geng, J.Z., Zhang, D.L., 2008. A precise U-Pb age on cassiterite from the Xianghualing tin-polymetallic deposit (Hunan, South China). Mineralium Deposita 43, 375–382.

Yuan, S.D., Peng, J.T., Hao, S., Li, H.M., Geng, J.Z., Zhang, D.L., 2011. In situ LA-MC-ICP-MS and ID-TIMS U-Pb geochronology of cassiterite in the giant Furong tin deposit, Hunan Province, South China: New constraints on the timing of tin-polymetallic mineralization. Ore Geology Reviews 43 (1), 235–242.

Zhang, Q., Jiang, Y.H., Wang, G.C., Liu, Z., Ni, C.Y., Qin, L., 2015. Origin of Silurian gabbros and I-type granites in central Fujian, SE China: Implications for the evolution of the early Paleozoic orogen of South China. Lithos 216–217 (6), 285–297.

Zhang, R., Lu, J., Lehmann, B., Li, C., Li, G., Zhang, L., Guo, J., Sun, W., 2017. Cassiterite U-Pb geochronology constrains magmatic-hydrothermal evolution in complex evolved granite systems: The classic Erzgebirge tin province (Saxony and Bohemia). Geology 45, 1095–1098.

Zhang, H., Lv, Z.H., Tang, Y., 2021. A review of LCT pegmatite and its lithium ore genesis. Acta Geological Sinica. 95 (10), 2955–2970. https://doi.org/10.19762/j.cnki. Dizhixuebao. 2021093 (in Chinese with English abstract).

Zhang, D., Wu, G.G., Di, Y.J., Wang, C.M., Yao, J.M., Zhang, Y.Y., et al., 2012. Geochronology of diagenesis and mineralization of the Luoyang Iron Deposit in Zhangping City, Fujian Province and its geological significance. Earth Sci. J. China Univ. Geosci. 37, 1217–1231. https://doi.org/10.3799/dqkx.2012.130. In Chinese with English abstract.

Zhang, H., 2001. The Geochemical Behaviors and Mechanisms of Incompatible Trace Elements in the Magmatic-hydrothermal Transition System: A Case study of Altay No.3 Pegmatite, Xinjiang. Doctor Thesis. Insitute of Geochemistry, Chinese Academy of Science.

Zhao, G.C., Cawood, P.A., 2012. Precambrian geology of China. Precambrian Research 222–223, 13–54.

Zhao, X.L., Mao, J.R., Chen, R., Xu, N.Z., Zeng, Q.T., He, H.M., 2007. Zircon SHRIMP age and geochemical characteristics of the Caixi pluton in southwestern Fujian Province. Acta Petrol. Mineral. 26, 223-231 (In Chinese with English Abstract). Doi: 10.1631/jzus.2007.B0900.

Zhou, Q.F., Qin, K.Z., Tang, D.M., Wang, C.L., Tian, Y., Sakyi, P.A., 2015. Mineralogy of the Koktokay No.3 pegmatite, Altai, NW China: implications for evolution and melt-fluid processes of rare-metal pegmatites. European Journal of Mineralogy 27, 433–457.

Zhou, Q.F., Qin, K.Z., Tang, D.M., Wang, C.L., Patrick, A.S., 2018. LA-ICP-MS U-Pb zircon, columbite–tantalite and ^{40}Ar-^{39}Ar muscovite age constraints for the rare-element pegmatite dykes in Altai orogenic belt. NW China. Geological Magazine 155 (3), 707–728.

Zhou, Q.F., Qin, K.Z., Tang, D.M., 2021. Mineralogy of columbite-group minerals from the rare-elements pegmatite dykes in the East-Qinling orogen, central China: Implications for formation times and ore genesis. Journal of Asian Earth Sciences 218, 104879.

Zhou, X.M., Sun, T., Shen, W.Z., Shu, L.S., Niu, Y.L., 2006. Petrogenesis of Mesozoic granitoids and volcanic rocks in South China: a response to tectonic evolution. Episodes 29 (1), 26–33.

Further reading

Černý, P., Ercit, T.S., 2005. The classification of granitic pegmatites revisited. The Canadian Mineralogist 43, 2005–2026.

Chew, D.M., Spikings, R.A., 2015. Geochronology and thermochronology using apatite: time and temperature lower crust to surface. Elements 11, 189–194.

Ercit, T.S., 1994. The geochemistry and crystal chemistry of columbite-group minerals from granitic pegmatites, southwestern Grenville province. Canadian Shield. Canadian Mineralogist. 32, 421–438.

Zhou, Z.H., Che, H.W., Ma, X.H., Gao, X., 2016. A preliminary discussion on some important advances of the rare metal deposit. Geology and Exploration 52 (4), 614–626 in Chinese with English abstract.